



Carbon Oxidation State in Microbial Polar Lipids Suggests Adaptation to Hot Spring Temperature and Redox Gradients

Grayson M. Boyer^{1*}, Florence Schubotz², Roger E. Summons³, Jade Woods⁴ and Everett L. Shock^{1,5}

¹ School of Earth and Space Exploration, Arizona State University, Tempe, AZ, United States, ² MARUM and Department of Geosciences, University of Bremen, Bremen, Germany, ³ Department of Earth, Atmospheric and Planetary Science, Massachusetts Institute of Technology, Cambridge, MA, United States, ⁴ Department of Chemistry, University of Nebraska-Lincoln, Lincoln, NE, United States, ⁵ School of Molecular Sciences, Arizona State University, Tempe, AZ, United States

OPEN ACCESS

Edited by:

Akihiko Yamagishi,
Tokyo University of Pharmacy and Life
Sciences, Japan

Reviewed by:

Jeremy Dodsworth,
The California State University,
United States
Zackary J. Jay,
Montana State University,
United States

*Correspondence:

Grayson M. Boyer
gmboyer@asu.edu

Specialty section:

This article was submitted to
Extreme Microbiology,
a section of the journal
Frontiers in Microbiology

Received: 05 May 2019

Accepted: 31 January 2020

Published: 20 February 2020

Citation:

Boyer GM, Schubotz F, Summons RE,
Woods J and Shock EL (2020)
Carbon Oxidation State in Microbial
Polar Lipids Suggests Adaptation to
Hot Spring Temperature and Redox
Gradients. *Front. Microbiol.* 11:229.
doi: 10.3389/fmicb.2020.00229

The influence of oxidation-reduction (redox) potential on the expression of biomolecules is a topic of ongoing exploration in geobiology. In this study, we investigate the novel possibility that structures and compositions of lipids produced by microbial communities are sensitive to environmental redox conditions. We extracted lipids from microbial biomass collected along the thermal and redox gradients of four alkaline hot springs in Yellowstone National Park (YNP) and investigated patterns in the average oxidation state of carbon (Z_C), a metric calculated from the chemical formulae of lipid structures. Carbon in intact polar lipids (IPLs) and their alkyl chains becomes more oxidized (higher Z_C) with increasing distance from each of the four hot spring sources. This coincides with decreased water temperature and increased concentrations of oxidized inorganic solutes, such as dissolved oxygen, sulfate, and nitrate. Carbon in IPLs is most reduced (lowest Z_C) in the hot, reduced conditions upstream, with abundance-weighted Z_C values between -1.68 and -1.56 . These values increase gradually downstream to around -1.36 to -1.33 in microbial communities living between 29.0 and 38.1°C . This near-linear increase in Z_C can be attributed to a shift from ether-linked to ester-linked alkyl chains, a decrease in average aliphatic carbons per chain (n_C), an increase in average degree of unsaturation per chain (n_{Unsat}), and increased cyclization in tetraether lipids. The Z_C of lipid headgroups and backbones did not change significantly downstream. Expression of lipids with relatively reduced carbon under reduced conditions and oxidized lipids under oxidized conditions may indicate microbial adaptation across environmental gradients in temperature and electron donor/acceptor supply.

Keywords: geobiochemistry, intact polar lipid, redox gradient, hydrothermal system, microbial community, carbon oxidation state

1. INTRODUCTION

There is ongoing interest in how geochemistry influences lipid compositions expressed in living communities of microorganisms. Lipids can provide valuable information about the environmental conditions experienced by the microbes that produced them (Summons and Walter, 1990; Pearson and Ingalls, 2013; Schouten et al., 2013). Structural diversity, longevity, and potential traceability

have led to the extensive use of lipids in biogeoscience as biomarkers (Summons et al., 1999; Brocks and Pearson, 2005; Schouten et al., 2007a). However, interpreting lipid biomarkers can be challenging because they are often not specific to any single type of organism or set of geochemical conditions (Rashby et al., 2007; Pitcher et al., 2009; French et al., 2015). For this reason, it is useful to investigate how bulk lipid compositions change across a variety of natural systems and then look for patterns that are universally applicable.

Hot spring outflow channels provide particularly accessible locations for studying changes in lipid composition across strong temperature and chemical gradients. For instance, microbial communities in the submerged sediments and biofilms of boiling springs tend to express lipid compositions substantially different from those in a hot spring photosynthetic microbial mat downstream (Zeng et al., 1992; Schubotz et al., 2013). It is conceivable that temperature is not the only environmental stress governing distributions of lipid structural adaptations along a hot spring outflow channel. As is often the case in hydrothermal systems, temperature gradients coincide with gradients in water chemistry, such as pH, salinity, solute concentrations, and redox potential. Changes in lipid structures and compositions along these gradients likely reflect adaptation to the collective set of environmental conditions experienced by the microorganisms present.

Our goal was to identify patterns in the properties of microbial lipids that might be influenced by redox geochemistry. We decided to explore the average oxidation state of carbon (Z_C) in lipids. In general, lower values of Z_C in a molecule represent more reduced carbon (e.g., -4 in CH_4) while higher values indicate more oxidized carbon (e.g., $+4$ in CO_2). Z_C was chosen as a metric primarily because thermodynamic or kinetic relationships with redox potential have been implicated in a variety of natural processes. Examples include the predicted energetic favorability of amino acids biosynthesis in submarine hydrothermal vents (Amend and Shock, 1998), preservation and degradation of organic matter in sediments and soils (Likens, 2010; LaRowe and Van Cappellen, 2011; Boye et al., 2017), oxidation rates of atmospheric organic aerosols (Kroll et al., 2011, 2015), and evolutionary convergence on proteomes inferred from metagenomes of microbial communities in natural systems (Dick and Shock, 2011, 2013; Dick, 2014; Dick et al., 2019; Fones et al., 2019), in aerobic and anaerobic nitrogen-fixing bacteria and archaea (Poudel et al., 2018), and in human cancer tissue (Dick, 2016, 2017). Further, several of these studies have implicated Z_C as a useful proxy for biosynthetic costs predicted from redox geochemistry (Amend and Shock, 1998; Dick and Shock, 2013; Dick et al., 2019). Thermodynamic properties do not exist for the full suite of lipid structures found along a hot spring outflow channel, so a similar assessment is not yet possible. However, we reasoned that if patterns in Z_C were evident, this would provide impetus for an eventual thermodynamic analysis to quantify lipid energy costs along thermal and chemical gradients.

We calculated Z_C values for intact polar lipids (IPLs) from eighteen sediment and microbial biomass samples collected from the outflow channels of four alkaline YNP hot springs: Bison Pool, Mound Spring, Empress Pool, and Octopus Spring. Further,

we calculated the Z_C of lipid headgroups, backbones, and alkyl chains to better understand how these components influence changes in the Z_C of IPLs. These Z_C values could then be correlated with the temperature, chemical composition, and redox state of the surrounding environment. We hypothesized that lipids sampled closest to the hot, reduced source of each spring would have the most reduced carbon on average, while the cool, oxidized conditions downstream would be characterized by lipids with more oxidized carbon. This general pattern aligns with observations of amino acid compositions inferred from metagenomes along the outflow channel of Bison Pool (Dick and Shock, 2011, 2013), and the strong correlations found between the Z_C of metagenomes and metatranscriptomes across natural redox gradients in a variety of microbial mats, terrestrial and marine hydrothermal systems, and hypersaline lakes (Dick et al., 2019). If compositions of microbial lipids display similar trends across a variety of natural systems, patterns in Z_C preserved in lipid biomarkers could potentially present a tantalizing target for inferring paleoredox.

2. METHODS

2.1. Water Chemistry

Temperature, conductivity, and pH were measured in the field as close to sampling locations as possible and before sample collection. Temperature and conductivity were measured with a YSI model 30 meter. Sample pH was measured with a WTW brand 3300i or 3110 model pH meter with WTW probe calibrated daily with pH 4, 7, and 10 buffer solutions at ambient temperature. Concentrations of dissolved oxygen and total sulfide were obtained from unfiltered water samples in the field using a Hach 2400 or 2800 portable spectrophotometer with Hach reagents and protocols. Water samples collected for laboratory analyses were filtered in the field with SuporTM (Pall Corporation) 0.2 μm polyethersulfone (PES) syringe filters into 30 mL HDPE Nalgene bottles and stored at -20°C . Concentrations of total ammonium, nitrate, nitrite, and sulfate were obtained by ion chromatography on two Dionex DX-600 systems; one for the analysis of cations and the other for anions. Suppressor columns on both systems were regenerated with deionized water to improve the signal-to-noise ratio. The anion analysis system was equipped with a potassium hydroxide eluent generator, carbonate removal device, and AS11-HC/AG11-HC columns. Columns were equilibrated with 5 mM hydroxide for 10 min before each injection. The injection volume was 100 μL for anions. Using a constant flow rate of 1.0 mL/min, the eluent hydroxide concentration was held isocratically at 5 mM for 5 min, then increased over the course of 31 min with a non-linear gradient (Chromleon curve 8). The cation analysis system was equipped with CS-16 and CG-16 columns. Cation samples were acidified with 6 N methanesulfonic acid (MSA) to 19 mM final concentration. The injection volume was 75 μL for cation analysis. The columns were eluted isocratically with 19 mM MSA and a flow rate of 0.5 mL/min. Ion concentrations were obtained by comparison to calibration curves created using mixed ion standards (Environmental Express, Charleston, SC, USA). Quantification accuracy was verified by the inclusion

of mixed ion-quality control standards (Thermo Scientific, Waltham, MA, USA) before, between, and after samples in each tray.

2.2. Sample Collection and Preparation

Samples for lipid analysis were collected with ethanol-cleaned spatulas or forceps into sterile 15 mL falcon tubes. Sediment and microbial mat samples were collected to ~1 cm depth, while samples BP1, BP2, and OS1 were taken from streamer biofilm communities clinging to gravel below the surface of the outflow water. Samples were frozen on dry ice in the field before storage in a -80°C freezer. Frozen samples were freeze-dried and homogenized with a sterile mortar and pestle. Lipid extractions were carried out using a modified version of the Bligh and Dyer procedure (White and Ringelberg, 1998). Briefly, 0.5–2 g sediment or 200–800 mg biofilm was dissolved in a mixture of methanol (MeOH), dichloromethane (DCM), and 50 mM phosphate buffer at pH 7.4 (2:1:0.8 v/v). The mixture was sonicated for 10 min and then centrifuged for 10 min at 2,000 rpm. The supernatant was collected and the remaining sediment or biofilm underwent one more extraction with the same solvent proportions, followed by two more times with a mixture of MeOH, DCM, and 50 mM trichloroacetic acid buffer at pH 2 (2:1:0.8) to aid extraction of glycerol dialkyl glycerol tetraether (GDGT) lipids (Nishihara and Koga, 1987), and one more time with a mixture of 3:1 DCM:MeOH to account for less polar lipids. A liquid-liquid extraction was performed by adding equal volumes of water and DCM to the pooled supernatant, which was then mixed and allowed to separate into aqueous polar and organic non-polar phases. The non-polar organic phase was collected and the remaining aqueous phase was washed with equal parts DCM for two additional rounds of liquid-liquid extraction. The resulting total lipid extract (TLE) was dried under N_2 and redissolved in 9:1 DCM and MeOH for later analyses.

2.3. HPLC-MS

Aliquots of the TLE were chromatographically separated on an Agilent 1200 series high-performance liquid chromatograph (HPLC) equipped with a Waters Acquity Ultra Performance Liquid Chromatography ethylene bridge hybrid (BEH) amide column according to the hydrophilic interaction chromatography (HILIC) method described in Wörmer et al. (2013). Mobile phases included solvent A, a mixture of acetonitrile, DCM, formic acid, and ammonia (750:250:0.015:0.15 v/v) and solvent B, a mixture of MeOH, H_2O , formic acid, and ammonia (500:500:4:4). The initial eluent was 99% solvent A and 1% solvent B that was brought to 5% B with a linear gradient over 4 min. The gradient continued to 25% B over 18.5 min, then to 40% over 0.5 min and held isocratically for 3.5 min. The flow rate was held constant at 0.4 mL min^{-1} throughout each run. Mass spectral analysis of IPLs was performed in positive ion mode on an Agilent 6520 Accurate-Mass Quadrupole Time-of-Flight (Q-TOF) mass spectrometer equipped with an electrospray ionization source.

2.4. Interpretation of Mass Spectra

IPLs were identified by the exact mass (M) of their parent ion, i.e., the intact lipid molecule with either a proton adduct $[M + \text{H}]^+$ or

ammonium ion adduct $[M + \text{NH}_4]^+$, and by comparing mass-to-charge (m/z) fragmentation patterns to previously published data as described in Sturt et al. (2004). **Table 1** summarizes references used for structural elucidation or mass spectral interpretation of IPLs. Structures exceeding the analytical window ($m/z > 2000$) were not detected, potentially leading to the exclusion of some higher molecular weight lipids.

While headgroup moiety identities, number of chains, backbone-chain linkage types, unsaturations, and aliphatic chain carbons were inferred based on mass spectra, other structural information was not obtained, such as positions of double bonds in alkyl chains or glycosidic bonds linking sugar headgroup moieties. Branching in non-isoprenoidal chains, such as those found in iso- and anteiso fatty acids, could not be determined from their straight-chain counterparts, necessitating “number of aliphatic carbons per chain” as a metric of alkyl chain carbon content rather than “chain length,” which implies distance spanned by straight or branching chains. Chain cyclizations in non-GDGT IPLs, such as cyclopropane fatty acids synthesized by certain bacteria (Grogan and Cronan, 1997), could not be discerned from unsaturations, as both types of chain modification have two fewer hydrogen atoms relative to a saturated straight chain. As such, these were counted as unsaturations. It is important to note that knowledge of the carbon positions of alkyl chain modifications, or whether a 2 Da loss is due to unsaturation or cyclization, and other fine details of molecular configuration are not required for the calculation of lipid Z_C . This is because Z_C depends solely on elemental abundances, oxidation states of non-carbon elements, and molecular charge. Additional discussion regarding IPLs potentially underrepresented in this study can be found in the **Supplementary Material**.

2.5. Lipid Quantification

IPLs were quantified based on manual peak integration of identified parent ions. The mole fraction of the i th IPL in a sample, x_i , was calculated using

$$x_i = \frac{I_i \cdot RF_i^{-1} \cdot m_i^{-1}}{\sum_i (I_i \cdot RF_i^{-1} \cdot m_i^{-1})}, \quad (1)$$

where I_i stands for the manually integrated MS peak area, RF_i indicates the assigned analytical response factor, and m_i designates the monoisotopic mass, all taken for the i th IPL parent ion.

Analytical response factors were applied in this study to partially account for differences in IPL ionization efficiency. Response factors were estimated by taking the linear slope of the injected masses vs. peak intensity for a small suite of co-analyzed commercially-available IPL standards. Because authentic standards are not available for every observed IPL structure, response factors were assigned based primarily on the similarity of headgroups to those of existing standards, under the assumption that headgroups are the chemical feature most likely responsible for differences in ionization efficiency among observed IPLs. For instance, Pendorf et al. (2013) found that response factors varied strongly between IPLs of

TABLE 1 | Observed polar lipids, headgroup formulae and their Z_C values, references used for identification, and assigned HPLC-MS quantification standards.

Headgroup			Backbone-chain linkage types*	Ref [†]	RF [§]	Headgroup			Backbone-chain linkage types*	Ref [†]	RF [§]
Abbreviation*	Formula [†]	Z_C				Abbreviation*	Formula [†]	Z_C			
Glycolipids						Phospholipids					
1G	C ₆ H ₁₁ O ₅	-0.166	DEG, AEG, DAG	a, b	1	APT	C ₅ H ₁₃ NO ₆ P	-0.600	DEG, AEG, DAG	a, b	3
			GDGT	b, c	2	DPG	C ₃ H ₈ O ₇ P ₂	-1.333	DAG	a	7
			CER	a, d	3	PC	C ₅ H ₁₄ NO ₃ P ⁺	-1.800	DAG	a, b	3
2G	C ₁₂ H ₂₁ O ₁₀	-0.083	DEG, AEG, DAG	a, b	4	PDME	C ₄ H ₁₁ NO ₃ P	-1.750	DAG	j	8
			GDGT	b, c	2	PE	C ₂ H ₇ NO ₃ P	-1.500	DAG, DEG, CER	a, c, d	9
3G	C ₁₈ H ₃₁ O ₁₅	-0.055	DEG, DAG	a	4	PG	C ₃ H ₈ O ₅ P	-1.000	DAG	a, b	10
			GDGT	b, c	2	PME	C ₃ H ₉ NO ₃ P	-1.666	DAG	j	11
2G-NACG-G	C ₂₄ H ₄₁ NO ₁₉	0.000	DAG, DEG	b, e	3	PS	C ₃ H ₇ NO ₅ P	0.333	DAG	a	12
3G-NACG-G	C ₃₀ H ₅₁ NO ₂₄	0.000	DEG	f	3	Aminolipids					
4G	C ₂₄ H ₄₁ O ₂₀	-0.042	GDGT	b, c	2	BL	C ₇ H ₁₅ NO ₂ ⁺	-1.000	DAG	b, k	13
GA	C ₆ H ₉ O ₆	0.500	DAG	g	1	OL	C ₅ H ₁₀ NO ₂	-0.600	FA-OH-FAm(-OH)	l, b, g	13
G-GA	C ₁₂ H ₁₉ O ₁₁	0.250	DAG	f	4	TM-KL	C ₉ H ₁₉ NO ₂ ⁺	-1.222	FA-OH-FAm	f	13
G-NG	C ₁₂ H ₂₂ NO ₉	-0.083	DAG, DEG	h	3	TM-OL	C ₈ H ₁₇ NO ₂ ⁺	-1.125	FA-OH-FAm(-OH)	m	13
NG-GA	C ₁₂ H ₂₀ NO ₁₀	0.250	DAG, AEG, DEG	f	3	Unidentified					
SQ	C ₆ H ₁₁ O ₇ S	-0.166	DAG	b	5	"223"	C ₇ H ₁₂ NO ₆	0.429	DAG	f	3
Glycophospholipids						Other					
1G-P	C ₆ H ₁₂ O ₈ P	-0.166	GDGT	b, c	2	hydroxyl "H"	H	Special	GDGT	b, c	2
2G-P	C ₁₂ H ₂₂ O ₁₃ P	-0.083	DEG	a, c	6						
			GDGT	b, c	2						
3G-P	C ₁₈ H ₃₂ O ₁₈ P	-0.055	GDGT	b, c	2						
G-MeNG-G-P	C ₁₉ H ₃₅ NO ₁₇ P	-0.158	DEG	f	3						
G-NG-G-P	C ₁₈ H ₃₃ NO ₁₇ P	-0.055	DEG	f	3						
MeNG-G-P	C ₁₃ H ₂₅ NO ₁₂ P	-0.231	DEG	f	3						
NACG-P	C ₁₂ H ₂₁ N ₂ O ₁₀ P	0.000	DAG, DEG	b, i	3						
NG-G-P	C ₁₂ H ₂₃ NO ₁₂ P	-0.083	DEG	f	3						
PI	C ₆ H ₁₂ O ₈ P	-0.166	DAG, AEG, DEG	a, b	6						
			CER	a, b, d	3						

*See text for abbreviations.

[†]Formulae correspond to elemental abundances contained in headgroups according to the division scheme depicted in **Figure 1** and described in the methods.

[‡]References used for structural elucidation and/or mass spectral interpretation; a. Sturt et al. (2004); b. Schubotz et al. (2013); c. Yoshinaga et al. (2011); d. Karlsson et al. (1998); e. Ferreira et al. (1999); f. this work (see **Supplementary Material** for mass spectral interpretation); g. Diercks et al. (2015); h. Schubotz et al. (2015); i. Yang et al. (2006); j. Wang et al. (2015); k. Benning et al. (1995); l. Zhang et al. (2009); m. Moore et al. (2013).

[§]IPL standard used to determine analytical response factors. Numbers correspond to commercially-available standards reported in **Table S1**.

^{||}This headgroup does not contain carbon and therefore does not have a Z_C value, though it still contributes to the Z_C calculated for all IPLs or headgroups in a sample.

different headgroups and less so from chain length during HPLC electrospray ionization.

Authentic standards and response factors are shown in **Table S1** and their assignments to observed IPLs are reported in **Table 1**. IPLs with headgroup analogs among standards include monoglycose (1G), diglycose (2G), sulfoquinovose (SQ), phosphatidylinositol (PI), diphosphatidyl glycerol (DPG), phosphatidylcholine (PC), phosphatidyl (N,N-dimethyl)ethanolamine (PDME), phosphatidylethanolamine (PE), phosphatidylglycerol (PG), phosphatidyl (N-methyl)ethanolamine (PME), and phosphatidylserine (PS). The rationale guiding response factor assignments for IPLs with no direct headgroup analog are briefly outlined below. IPLs with nitrogen-bearing groups, such as diglycosyl

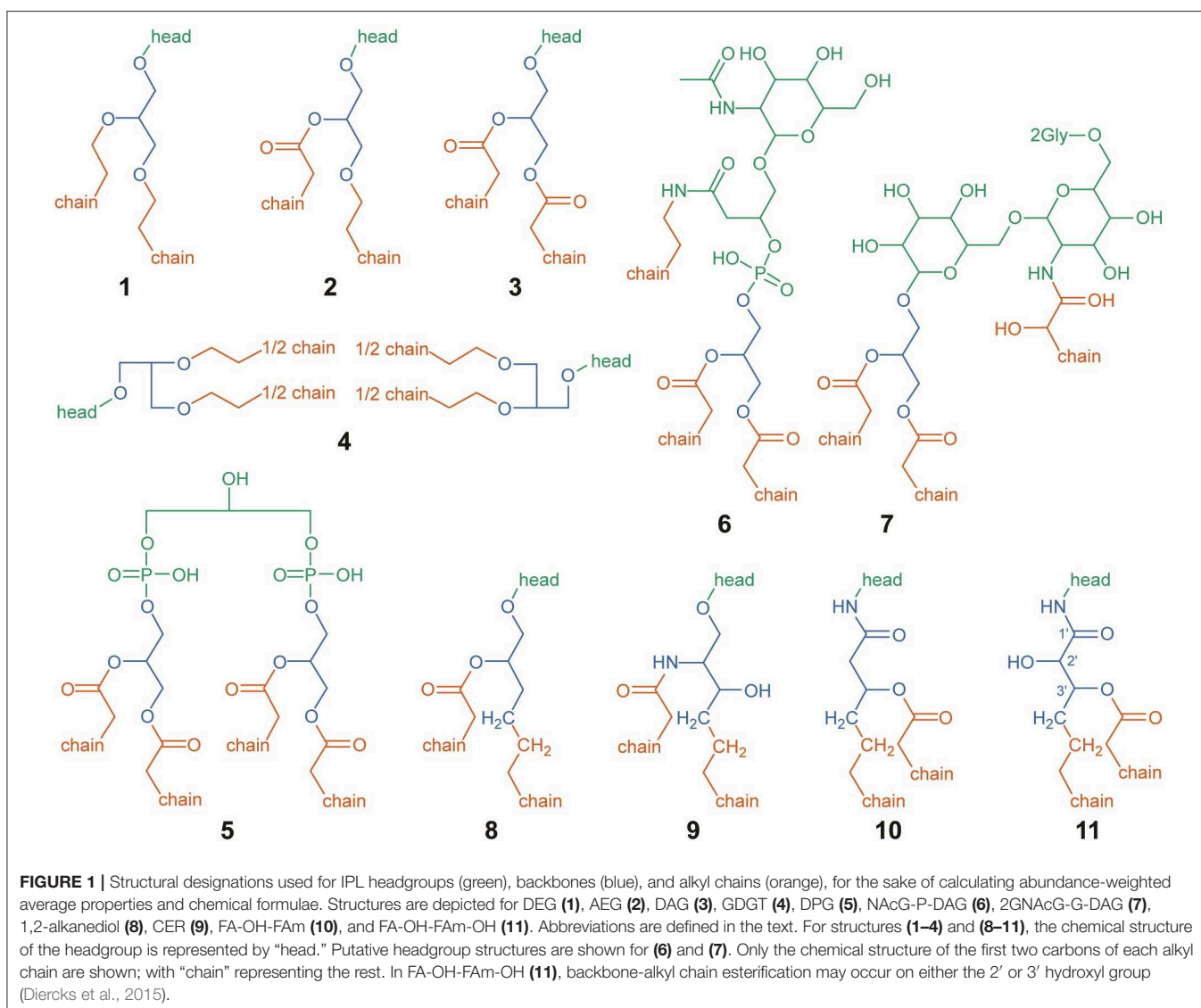
(N-acetyl)glycosaminyl glucose (2G-NACG-G), triglycosyl (N-acetyl)glycosaminyl glucose (3G-NACG-G), monoglycosyl (N)glycosamine (G-NG), (N)glycosaminyl glycoronic acid (NG-GA), glycosyl (N-methyl) glycosaminyl glycosyl phosphate (G-MeNG-G-P), glycosyl (N)glycosaminyl glycosyl phosphate (G-NG-G-P), (N-methyl)glycosaminyl glycosyl phosphate (MeNG-G-P), (N-acetyl)glycosaminyl phosphate (NACG-P), (N)glycosaminyl monoglycosyl phosphate (NG-G-P), aminophosphopentetetrol (APT), ceramide (CER) lipids, and lipids with an unidentified "223" headgroup (see **Figure S4**) were assigned the response factor obtained from C42:0 PC diacylglycerol (DAG), under the assumption that the nitrogen-bearing functional groups contained in these lipids might result in comparable ionization efficiencies. This assumption was

based on qualitative assessment of the differences in relative peak intensities of nitrogen-bearing and non-nitrogen bearing standards; the former had peak intensities that averaged about an order of magnitude greater than the latter (**Table S1**). Lipids with a glycoronic acid (GA) headgroup, a non-nitrogen-containing single-moiety glycosyl group, were assigned the response factor obtained from a 1G-DAG standard composed of a mixture of C34:2 and C34:3 chain lengths. Lipids with a monoglycosyl glycoronic acid (G-GA), triglycose (3G), or tetraglycose (4G) headgroup were assigned the response factor of the standard containing the closest number of non-nitrogen-bearing glycosyl moieties; a 2G-DAG standard mixture of C34:2, C34:3, and C36:6 chain lengths. Glycophospholipids with no nitrogen, such as monoglycosyl phosphate (1G-P), diglycosyl phosphate (2G-P) or triglycosyl phosphate (3G-P) headgroups, were assigned the response factor obtained from C32:0 PI-DAG. All GDGTs were assigned the response factor obtained from the 1G-GDGT-PG standard that included a mixture of H-shaped and non-H-shaped

alkyl chains with 0-3 internal rings. All aminolipids, including ornithine lipids (OL), monohydroxylated ornithine lipids (OL-OH), trimethylornithine lipids (TM-OL), monohydroxylated trimethylornithine lipids (TM-OL-OH), trimethyllysine lipids (TM-KL) and betaine lipids (BL), were assigned the response factor obtained from C32:0 1,2-dipalmitoyl-*sn*-glycero-3-O-4'-[*N,N,N*-trimethyl(d9)]-homoserine (DGTS-d9) based on structural similarities of their amino acid headgroups.

2.6. IPL Structural Designations and Chemical Formulae

Headgroups, backbones, and alkyl chains serve as the three basic building blocks comprising IPL structure, each with its own set of observed structural variations. The schematic used to categorize divisions among observed headgroup-backbone-alkyl chain variation is shown in **Figure 1**, with green, blue, and orange portions indicating headgroup, backbone, and alkyl chain structures, respectively. When considering differences across



widely varying lipid structures, it is important to define strict boundaries between components for the sake of consistently comparing properties that depend on chemical formulae, such as Z_C or the number of aliphatic carbons in an alkyl chain. This is particularly important for comparing lipids with glycerol backbones to those without. Generalized lipid structures with glycerol backbones considered in this study include diether glycerol (DEG, **1**), mixed acyl/ether glycerol (AEG, **2**), diacyl glycerol (DAG, **3**), GDGT (**4**), DPG (**5**), and putative structures NAcG-P (**6**, DAG variant shown), 2GNAcG-G (**7**, DAG variant shown), and 3GNAcG-G-DEG (**Figure S7**). Structures that do not contain a glycerol backbone include 1,2-alkanediols (**8**), CER lipids (**9**), fatty acid esters of hydroxy fatty amides (FA-OH-FAM, **10**), and monohydroxylated FA-OH-FAM lipids (FA-OH-FAM-OH, **11**).

The headgroup of an IPL was structurally designated as one or more covalently bonded polar moieties linked to one or more backbones, represented by green structures in **Figure 1**. In some cases, the headgroup itself may be directly linked to one or more alkyl chains, such as in structures **6** and **7**. The chemical formulae of all headgroups reported in **Table 1** are assumed to be protonated to an extent that results in a neutrally-charged IPL, though it should be noted that Z_C is not affected by pH-dependent ionization. The +1 charge imparted by a quaternary ammonium functional group is not the result of pH-dependent ionization and therefore affects Z_C , which is why this charge is included in the chemical formulae of PC, TM-OL, TM-OL-OH, and TM-KL.

Most IPL structures observed in this study have one mole of headgroup per mole of lipid with the exception of GDGTs, which has two. It has been shown that sugar and phosphate moieties can be distributed between the two headgroups of a GDGT, resulting in a variety of possible isomers (Yoshinaga et al., 2011). In this study, we could determine the total number and type of moieties among the two headgroups of GDGTs but the analytical method did not allow us to determine headgroup positions. For instance, the two hexose moieties in 2G-GDGT may be clustered on one end of the lipid or evenly distributed among both ends. Our definition of an IPL headgroup was chosen to ensure consistency in headgroup chemical formulae regardless of position. All configurations of headgroup moieties in 2G-GDGT, for example, have the same total elemental abundance. A 2G-GDGT with two monoglycosyl headgroups, each with the formula $C_6H_{11}O_5$, has a total elemental abundance of $C_{12}H_{22}O_{10}$ among headgroups. If the 2G-GDGT has one diglycosyl headgroup with the formula $C_{12}H_{21}O_{10}$, then its other headgroup must be a single hydrogen atom to bring the total to $C_{12}H_{22}O_{10}$. In GDGTs with every headgroup moiety clustered on one side, this hydrogen atom is defined as belonging to the hydroxyl group on the opposite end of the GDGT, and is listed as its own headgroup in **Table 1**.

Lipid backbones are designated by the blue structures in **Figure 1**. Most IPLs observed in this study have one mole of backbone per mole of lipid. However, GDGT (**4**) and DPG (**5**) lipids were counted as having two moles of backbone per mole of lipid. IPL backbones were structurally designated according to two criteria chosen to promote consistency among observed IPL structures. First, the backbone must have a

linear aliphatic chain of three carbons. Second, the backbone must include three “connector” functional groups that serve to anchor the headgroup and alkyl chains. In addition to these three connector groups, the three-carbon backbone may include modifications like hydroxylations or carbonyl groups. Various backbone-alkyl chain linkage types are shown in **Figure 2**, with backbone connector groups shown proximal to the R_1 group representing the rest of the backbone; a methylene group (CH_2) for a carbon-carbon (C-C) link (**12**), an oxygen atom ($-O-$) for an ether link (**13–16**), $-NH-$ for an amide link (**17**), or an oxygen atom ($-O-$) for an ester link (**18–21**). Connector groups were included in the structure of the backbone rather than in the alkyl chain to maintain consistency when calculating n_C in alkyl chains with C-C backbone-chain linkage relative to other chains. To demonstrate, consider the C-C linked alkyl chain (**12**) and the ether-linked alkyl chain (**13**) in **Figure 2**. Both are saturated and have approximately the same physical length. To ensure that both chains have the same value for n_C , the connector groups proximal to R_1 must be categorized as part of the backbone. Structures **8** through **11** illustrate how the backbone contains one CH_2 group (in blue) and the alkyl chain contains the other (in orange) in a C-C link.

Alkyl chains are aliphatic hydrocarbon chains linked to the IPL backbone or in some cases, directly to the headgroup. Their designation is indicated by orange structures in **Figure 1**. Alkyl chains begin at the carbon atom directly after the backbone “connector” atom and continue to the distal methyl group that caps the end of the chain. Most of the IPL structures observed in this study had two moles of alkyl chains per mole of lipid (**1–3**, **8–11**), though some had three (**6–7**) or four (**4–5**). Each GDGT had two membrane-spanning biphytanyl alkyl chains with forty carbons apiece. GDGT chains were conceptually divided into twenty-carbon half-chains to permit averaging of chain properties, such as Z_C and n_C , between GDGTs and non-GDGT bilayer lipids. Therefore, one mole of GDGT was counted as having four moles of half-chains (see Structure **4**) so that they could be more directly compared to the alkyl chains of non-GDGTs. GDGT half-chains terminate in a methylene group (CH_2) that is covalently bonded to the methylene group of another GDGT half-chain within the membrane interior (e.g., Structures **15** or **16**).

2.7. Calculation of Average Lipid Properties and Elemental Composition

Abundance-weighted properties of IPL headgroups, backbones, and chains were calculated for each sample using the equation

$$\Xi = \frac{\sum_i \Xi_{ipl,i} \cdot x_i}{\sum_i n_{component,i} \cdot x_i}, \quad (2)$$

where Ξ indicates the average property of interest (e.g., average n_C of IPLs in a sample), $\Xi_{ipl,i}$ represents the property summed across all components of the same type in the i th IPL (e.g., 32 carbons in the alkyl chains of a C32 IPL) with $n_{component,i}$ instances of the component in the IPL (e.g., 2 alkyl chains in

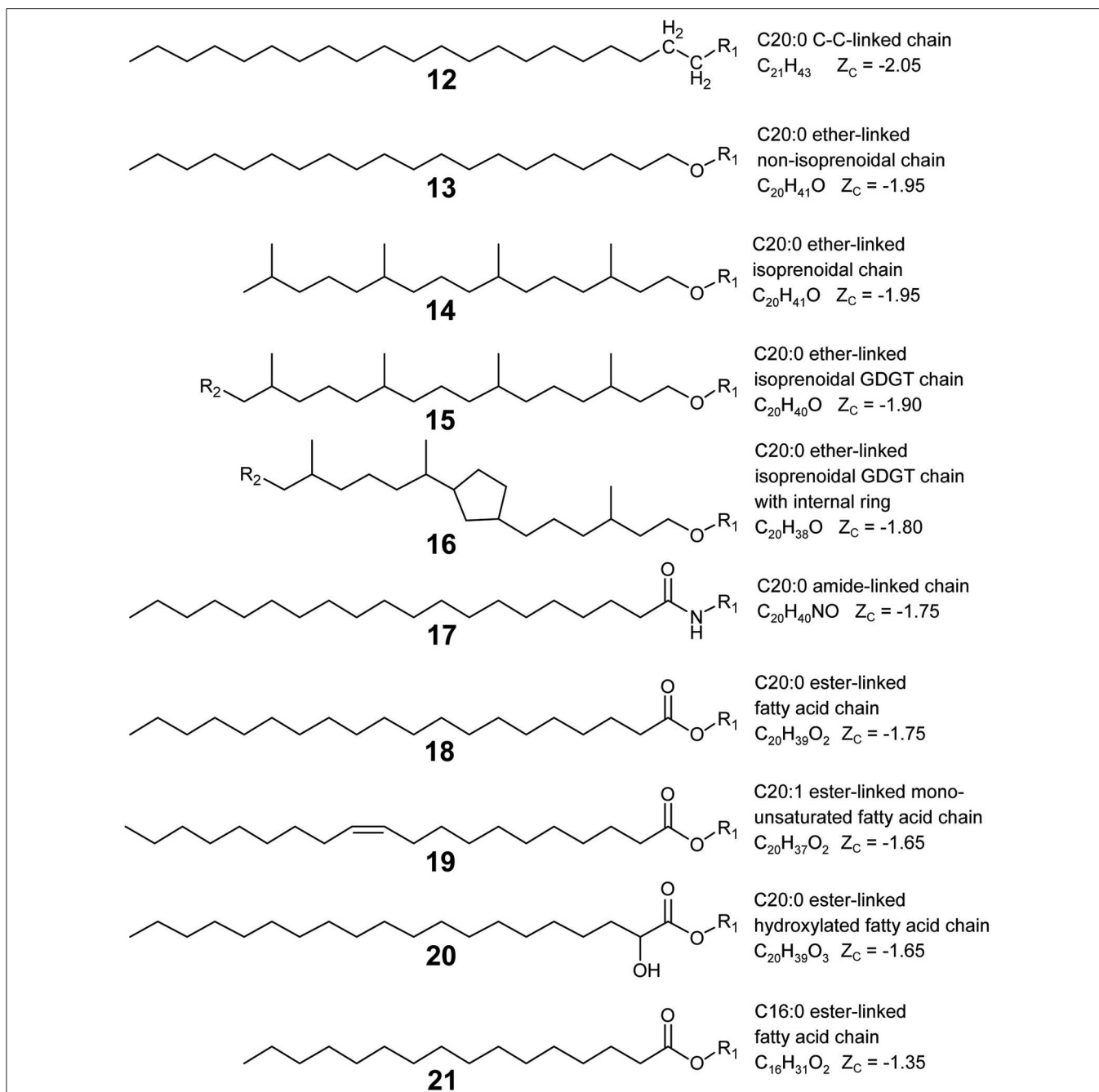


FIGURE 2 | Lipid alkyl chain modifications and backbone-chain linkage types organized by Z_C from reduced (top) to oxidized (bottom). Example structures were chosen to permit comparison of Z_C between various types of alkyl chain modifications: chain-backbone linkage type as C-C (**12**), ether (**13**), amide (**17**), or ester (**18**); non-branching and branching chains (**13**, **14**); isoprenoidal non-GDGT chains and GDGT half-chains (**14**, **15**); GDGT half-chains without and with an internal ring (**15**, **16**); saturated and unsaturated chains (**18**, **19**); non-hydroxylated and hydroxylated chains (**18**, **20**); and chains with a greater and lesser number of aliphatic carbons (**18**, **21**). R_1 represents a covalent bond to the rest of the lipid, and R_2 indicates a covalent bond with another GDGT half-chain.

a DAG IPL). Finally, x_i represents the mole fraction of the i th IPL. Abundance-weighted properties calculated in this way include nC, nUnsat, and the number of hydroxylations (nOH) per alkyl chain, the fraction of alkyl half-chains belonging to GDGT (x_{GDGT}), and the fraction backbone-alkyl chain linkage

types with an ether (x_{ether}), ester (x_{ester}), amide (x_{amide}), or C-C (x_{C-C}) bond. The abundance-weighted number of internal rings per GDGT (not per alkyl chain) in a sample was also calculated using Equation (2) by setting x_i to the mole fraction of the i th GDGT (rather than the i th IPL), and setting $n_{component,i}$

equal to one, thereby producing a per-GDGT property and not a per-chain property.

Average chemical formulae of IPLs and their component parts were also calculated for each sample using Equation (2) by substituting $\Xi_{ipl,i}$ with charge and elemental abundances of carbon, hydrogen, nitrogen, oxygen, phosphorus, and sulfur atoms in the i th IPL. The value of $n_{component,i}$ was set to one when calculating average chemical formulae of full IPLs. Even when the structure of an IPL or component is unclear, its elemental composition is typically obtainable with high resolution accurate-mass mass spectrometry. This permits the inclusion of ambiguous structures when calculating average chemical formulae. For example, the unidentified “223” headgroup is suspected to have the chemical formula $C_7H_{12}NO_6$ based on mass spectral interpretation (Figure S4) and could therefore be included in the calculation of average chemical formulae of IPLs and headgroups.

2.8. Calculation of IPL Z_C

A step-by-step example illustrating how lipid Z_C can be calculated for a hypothetical sample is provided in the **Supplementary Material**. The Z_C of IPLs and their component parts were calculated using the equation

$$Z_C = \frac{2o + 3n - 5p - 4s - h + Z}{c}, \quad (3)$$

where Z stands for the net charge and c , h , n , o , p , and s represent the number of atoms of carbon, hydrogen, nitrogen, oxygen, phosphorus, and sulfur in the chemical formula of interest. Hydrogen, oxygen, and nitrogen were assigned oxidation states of +1, -2, and -3. Sulfur within the sulfonic acid group of SQ-DAG was assigned an oxidation state of +4. Phosphorus was assigned an oxidation state of +5 to be consistent with that of phosphorus within the phosphate ion. Charge gained or lost by pH-dependent protonation or deprotonation, as is common in many lipid headgroups, does not affect Z_C .

Equation (3) was used to determine the Z_C values of individual lipid structures, such as those reported in Figure 2. It was also used to calculate abundance-weighted Z_C values in each sample; in this case, using the abundance-weighted charge and carbon, hydrogen, nitrogen, oxygen, phosphorus, and sulfur atoms in the average chemical formulae of IPLs and their components.

2.9. Statistical Simulation of Analytical Uncertainty

We conducted a statistical analysis to check whether observed trends in Z_C were not an artifact of the methods chosen for IPL quantification. To do this, we employed an R script to carry out a Monte Carlo-style bootstrap sensitivity analysis in which manually integrated IPL HPLC-MS peak areas were allowed to vary randomly by up to 30% of their original value over 999 iterations. In addition, the analytical response factors applied to any headgroup-backbone combination listed in Table 1 were allowed to vary by up two orders of magnitude higher and lower. Z_C for lipids and their components were re-calculated from average chemical formulae after each iteration.

3. RESULTS AND DISCUSSION

3.1. Hot Spring Sample Sites

Temperature, pH, and conductivity measurements are shown in Table 2 for samples taken along the outflow channels of Bison Pool, Mound Spring, Empress Pool, and Octopus Spring. Upstream samples collected closest to the source pools of each spring ranged from circumneutral to alkaline (pH 5.78–8.81), with temperatures close to the boiling point of water (82.2–91.0°C) given their altitude in YNP (~2,200 m above sea level at Bison Pool and Mound Spring, 2,250 m at Octopus Spring, and 2,300 m at Empress Pool). Water temperature decreased and pH increased with distance from the source, with the furthest samples downstream ranging between 29.0 and 59.8°C and pH 8.27 and 9.53. Trends in conductivity were typically non-linear and were not shared among hot springs.

Microbial communities inhabiting the sediment below the surface of the water changed visibly downstream. At Bison Pool and Octopus Spring, upstream samples contained white or pink streamer biofilm communities (SBCs) clinging to submerged pebbles or mineral protrusions. A study by Meyer-Dombard et al. (2011) found the bulk of the bacterial community in the pink streamers of Bison Pool belonged to *Aquificales* and *Thermatogales*, while most archaea were mainly comprised of *Crenarchaeota* and *Desulfurococcales*. SBCs were absent at Empress Pool and Mound Spring, despite the latter's proximity and apparent geochemical similarity to Bison Pool. Communities of photosynthetic microorganisms were visually identified in downstream samples by their pigmentation. At Bison Pool, Mound Spring, and Octopus Spring, the transition from chemotrophic to mixed photo/chemo-trophic microbial communities could be readily identified by the sharp onset of photosynthetic pigmentation over a span of a few centimeters. This transition at Empress Pool was not as distinct, and visual confirmation of samples with phototrophic communities relied on faint patches of pigmented microorganisms. The maximum temperature we observed for phototrophic organisms was at 73.3°C at BP3, which falls close to the maximum temperature limit observed for photosynthesis among alkaline YNP hot springs reported by Cox et al. (2011).

Downstream from the “photosynthetic fringe,” laminated green/orange photosynthetic mats were present at Bison Pool, Mound Spring, and Octopus Spring. Previous work by Ward et al. (1987) at Octopus Spring and Meyer-Dombard et al. (2011) at Bison Pool and Mound Spring showed that *Synechococcus* cyanobacteria and *Chloroflexus* bacteria comprise the bulk of the community at these mats. Empress Pool did not have a massive laminar microbial mat, though green/orange photosynthetic communities were visually apparent along either side of the channel in broken patches downstream. Samples BP6 and MS5, taken from post-mat runoff zones of gray-beige flocculent matter, were identified as hosting photosynthetic microbes based on visual confirmation of green pigmentation within the floc.

Microbial mats like those found at Bison Pool, Mound Spring, and Octopus Spring are complex stratified ecosystems of interconnected metabolic cycles. The oxic conditions measured in the water column and upper mat give way to anoxia after

TABLE 2 | Selected geochemical and physical data from each sample site.

Site	Sample	12T UTM coordinates		Dist ^a (m)	Zone ^b	Temperature (°C)	pH	Conductivity ^c (μS/cm)
		Easting	Northing					
Bison	BP1	510710	4935155	2.9	C	89.0	7.23	1550
Pool	BP2	510715	4935156	8.2	C	80.9	7.34	1568
	BP3	510718	4935157	11.1	T	73.3	7.27	1540
	BP4	510719	4935159	13.4	P	63.1	8.09	— ^d
	BP5	510719	4935163	17.2	P	40.5	8.25	1508
	BP6	510724	4935165	22.6	P	29.0	9.01	1697
	Mound	MS1	511114	4934621	3.6	C	91.0	8.81
Spring	MS2	511108	4934624	12.7	C	77.3	8.65	1621
	MS3	511098	4934628	24.2	P	64.8	9.08	1617
	MS4	511083	4934621	38.7	P	53.0	9.22	1634
	MS5	511049	4934625	53	P	35.1	9.53	1660
	Empress	EP1	0521589	4948280	2.2	C	82.2	5.78
Pool	EP2	0521585	4948280	6.2	T	70.5	6.96	1832
	EP3	0521580	4948285	13.3	T	60.7	7.63	1840
	EP4	0521560	4948293	34.8	P	51.6	7.99	1860
	EP5	0521558	4948295	37.6	P	38.1	8.42	1664
	Octopus	OS1	0516054	4931217	7.0	C	85.4	7.29
Spring	OS2	0516016	4931212	38.3	P	59.8	8.27	1581

^aDistance from hot spring source.

^bMajor metabolic regime representative of the microbial community at the sample site, interpreted visually in the field based on the presence or absence of photosynthetic pigments; C, strictly chemosynthetic; T, transition to phototrophy; P, photosynthetic.

^cConductivity was normalized to 25 °C using the formula $Cond_{25}/(1 + \alpha(T - 25))$, where $Cond_T$ stands for the conductivity measured at the temperature of the sample site and α represents the temperature correction coefficient taken as 0.02 for freshwater.

^dNo data.

only a few millimeters depth (Dupraz and Visscher, 2005; Franks and Stolz, 2009). Further, redox conditions in a microbial mat have been shown to undergo extreme fluctuations throughout a 24-h period (Fenchel, 1998; Visscher et al., 1998; Jonkers et al., 2003). The upper few millimeters of a mat are supersaturated with O₂ from cyanobacterial photosynthesis during the day and anoxic within minutes to hours of darkness. In this study, we strove to minimize the influence of sunlight availability, diel cycles, and other complicating factors arising from the passage of time by collecting samples at each outflow channel during light hours of the same day. In this way, we sought to capture a snapshot of water chemistry and lipid profiles from which to draw broad correlations. There is an intriguing possibility of steep biogeochemical gradients coinciding with substantial changes in lipid composition across a depth of millimeters, though these would have been interpreted as bulk averages according to our sampling method.

3.2. Water Chemistry

Measured concentrations of dissolved oxygen, nitrate, nitrite, sulfate, total ammonia, and total sulfide are given in Table 3. In all four outflow channels, concentrations of dissolved oxygen were lowest in samples closest to the source and increased downstream. This could be attributable to a combination of factors, such as extent of mixing with atmospheric O₂, input

from microbial oxygenic photosynthesis, and concentration via evaporation. Sulfate concentrations also increased downstream and coincided with decreasing sulfide concentrations, as shown in Figure 3. A previous experiment by Cox et al. (2011) concluded that abiotic processes, such as degassing, oxidation by O₂ and hydrogen peroxide, and mineral precipitation were too slow to explain the downstream decrease in sulfide concentration at Bison Pool, and that oxidation of sulfide by outflow channel microorganisms was likely responsible. It is feasible that biological oxidation of sulfide may also be occurring in the outflow channels of Mound Spring, Empress Pool, and Octopus Spring given the parallels in geochemistry observed among these springs. In addition to sulfide and sulfate, we observed an inverse correlation between ammonia and nitrate concentrations, with the highest concentrations of ammonia closest to the source and decreasing downstream while nitrate concentrations steadily increase (Table 3). Oxidation of ammonia into nitrite and nitrate by microbial communities via nitrification is one possible explanation. However, previous phylogenetic and metagenomic studies of nitrogen-cycling genes in Bison Pool and Mound Spring microbial communities have found either an absence of genes involved in ammonia oxidation (Swingley et al., 2012), or limited presence with no active expression (Loiacono, 2013). Regardless of the cause, depletion of sulfide and ammonia coinciding with an increase in sulfate,

TABLE 3 | Concentrations of selected redox-sensitive dissolved chemical species^a.

Site	Sample	Oxidized				Reduced	
		O ₂ (mg l ⁻¹)	NO ₃ ⁻ (mg l ⁻¹)	NO ₂ ⁻ (mg l ⁻¹)	∑SO ₄ ²⁻ (mg l ⁻¹)	∑NH ₄ ⁺ (mg l ⁻¹)	∑HS ⁻ (μg l ⁻¹)
Bison	BP1	0.2	0.01	0.02	13.11	0.07	230
Pool	BP2	0.7	0.01	0.04	15.43	0.06	220
	BP3	1.1	0.02	0.01	16.81	0.04	bdl ^b
	BP4	2.3	0.03	0.02	16.50	0.02	6
	BP5	5.7	0.004	bdl	17.18	0.01	15
	BP6	3.3	0.07	bdl	18.32	0.02	10
	Mound	MS1	0.4	0.01	bdl	14.33	0.07
Spring	MS2	2.2	0.01	bdl	15.03	0.01	758
	MS3	1.4	0.04	0.02	16.99	0.03	236
	MS4	3.6	0.02	0.01	17.56	0.02	70
	MS5	6.9	0.06	bdl	20.11	bdl	bdl
	Empress	EP1	0.4	0.01	0.08	106.87	0.42
Pool	EP2	0.7	– ^c	–	–	–	97
	EP3	1.2	0.01	bdl	106.70	0.31	37
	EP4	1.3	0.03	0.03	111.70	0.39	31
	EP5	3.4	0.08	0.01	111.24	0.14	18
	Octopus	OS1	0.5	0.03	0.03	17.82	0.06
Spring	OS2	3.3	0.03	0.02	18.76	0.02	12

^aSulfide (HS⁻), ammonium (NH₄⁺), and sulfate (SO₄²⁻) concentrations are summed for their respective pH-dependent protonated states.

^bbdl: below detection limit.

^cNo data.

nitrate, and dissolved oxygen suggests that water is most reduced at the source and becomes increasingly oxidized downstream along these hot spring outflow channels. This would agree with previous oxidation-reduction potential (ORP) Ag/AgCl electrode measurements that confirmed a downstream increase in Eh along the outflow channels of Bison Pool and Mound Spring (Dick and Shock, 2011).

3.3. IPL Headgroup and Backbone Distributions

Mole fractions of IPLs grouped according to their headgroup/backbone combinations and color-coded by their suspected source organisms are shown in **Figure 4**. Archaeally-derived GDGT and archaeol (AR) lipids (**Figure 4**, blue bars 1–5) were most abundant in samples collected closer to the source of each hot spring. MS1 and EP1 were the only two samples where archaeal lipids outnumbered those of non-archaea. Considering that one mole of GDGT is functionally equivalent to two moles of non-GDGTs in a membrane bilayer (in a general sense), it is unsurprising that archaeal membranes comprise the majority of lipids in the hottest upstream samples where Archaea are expected to thrive (Barns et al., 1994, 1996; Meyer-Dombard et al., 2005; Schouten et al., 2007b; Zhang et al., 2008). 1G-GDGT was found in >2% abundance in all but five samples and was always more abundant than any other archaeal lipid except

for 2G-P-AR in sample OS1. Upstream samples were typically rich in lipids thought to be diagnostic of members of *Aquificae* bacteria (**Figure 4**, red bars 6–9), including PI-DEG/AEG and APT-DEG/AEG (Sturt et al., 2004; Schubotz et al., 2013). Indeed, previous phylogenetic analyses have confirmed the presence of *Aquificae* in the SBCs of Bison Pool and Octopus Spring, and in the high-temperature sediments of Mound Spring, and Empress Pool (Reysenbach et al., 1994; Meyer-Dombard et al., 2005, 2011; Spear et al., 2005; Swingley et al., 2012; Schubotz et al., 2013; Beam et al., 2016; Colman et al., 2016; Romero, 2018). SQ-DAG lipids found in the photosynthetic membranes of cyanobacteria and other phototrophs (Sato, 2004) were located in mid-to-downstream samples where green/orange pigments were visually confirmed in microbial communities (**Figure 4**, green bar 10). These sites also hosted an abundance of other lipids common in, but not specific to, phototrophic membranes, such as DAG lipids with 1G, 2G, and PG headgroups (Murata and Siegenthaler, 1998).

Glycolipids were abundant in every sample (**Figure 4**, yellow bars 11–22), with mole fractions ranging from 31% in OS2 to nearly 100% in MS1. Glycophospholipids (**Figure 4**, yellow bars 23–24), especially PI-DAG, were also abundant in nearly every sample and reached up to 63% in OS2. This preponderance of glyco(phospho)lipids is thought to confer heat tolerance via inter-lipid hydrogen bonding (Curatolo, 1987). Evidence to support this hypothesis comes from experiments by Adams et al. (1971), Ray et al. (1971), and Prado et al. (1988) demonstrating that higher growth temperatures result in a greater proportion of glycolipids to other membrane lipids in various thermophilic microorganisms.

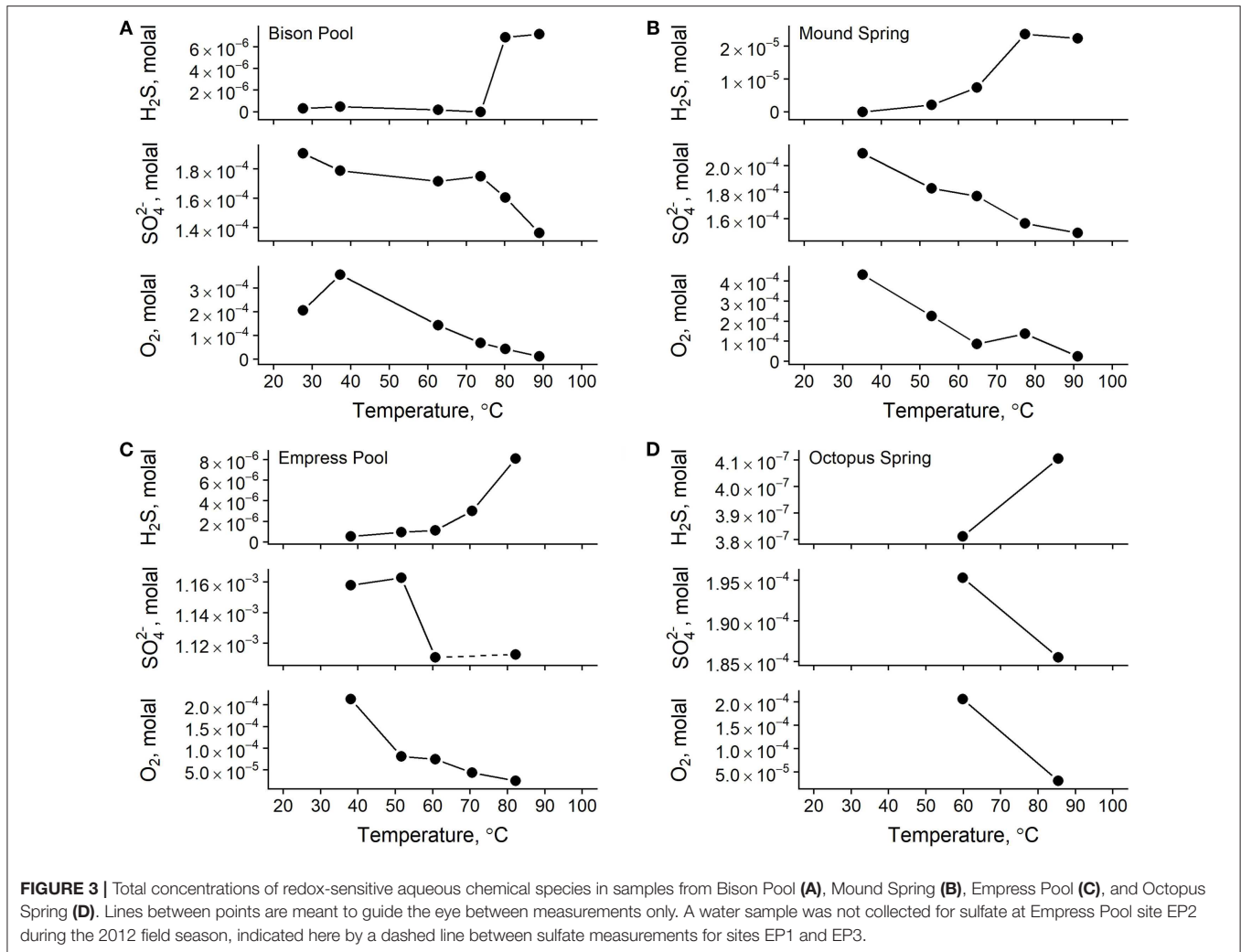
Downstream samples collected from Bison Pool, Mound Spring, and Empress Pool featured many DAG phospholipids common to unspecific Bacteria and Eukaryotes (**Figure 4**, yellow bars 25–31), such as DPG, PC, PE, PG, PME, and PS (Kent, 1995; López-Lara and Geiger, 2017). These lipids were not abundant in Octopus Spring sample OS2, possibly because the temperature measured at this sample site, 59.8°C, roughly corresponds to the upper temperature limit of about 60°C reported for Eukaryotes (Tansey and Brock, 1972). Aminolipids (**Figure 4**, yellow bars 32–34) were less abundant upstream (typically <2%) than in downstream samples, where they reached up to 19% in sample EP5. IPLs bearing a headgroup with an exact mass consistent with the formula of C₇H₁₂NO₆, referred to here as “223-DAG” (**Figure 4**, purple bar 35), were most abundant (2–3%) in samples collected between 40 and 53°C. The structure and source of this lipid is unknown.

3.4. IPL Alkyl Chain Properties

Changes in abundance-weighted average properties of microbial IPL alkyl chains were observed downstream in all four outflow channels (**Table S2**). Patterns in chain-backbone linkage, aliphatic carbon number, degree of unsaturation and GDGT cyclization, and chain hydroxylations are described below.

3.4.1. Chain-Backbone Linkage

As shown in **Figure 5**, upstream samples from all four hot spring outflow channels are dominated by ether-linked alkyl chains



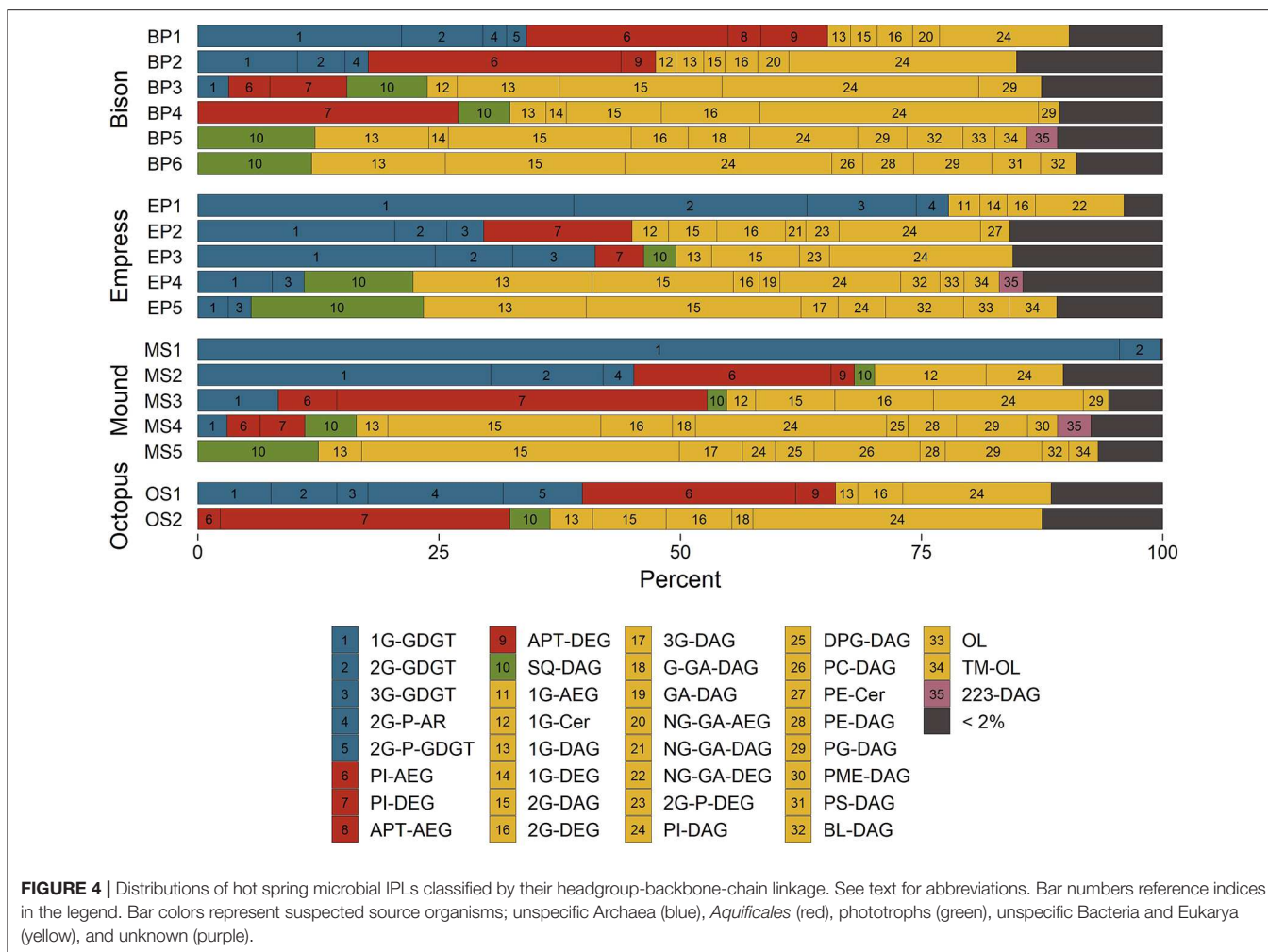
(70% mole fraction at BP1 to nearly 100% at MS1). Ether-linked alkyl chains are resistant to hydrolysis (Daniel and Cowan, 2000). The proportion of ether-linked chains decreases downstream from each hot spring source, giving rise to a growing proportion of ester-linked chains. The onset of photosynthetic communities coincides with a sharp increase in the proportion of ester-linked chains, comprising over 50% of alkyl chains in all samples containing visible photosynthetic pigmentation. Downstream samples have the highest abundance of ester-linked chains in each outflow channel (81–97% in samples below 40°C). Chains linked to the backbone via an amide or C–C bond are also present, though in relatively low abundance (<5% in any sample).

While ether lipids are the common chain-backbone linkage in archaea, they are a rare occurrence in bacteria. Bacterial ether lipids are predominantly reported from thermophilic bacteria (Huber et al., 1992; Jahnke et al., 2001). However, few mesophilic organisms are also able to synthesize these lipids in culture (Vinçon-Laugier et al., 2017). Contrasting these sparse culturing reports, bacterial ether lipids are abundantly found in the environment, typically under anoxic conditions, such as stratified water columns and marine sediments (Schubotz

et al., 2009; Schröder, 2015; Evans et al., 2017). Based on these reports, temperature is not the only environmental variable influencing the distribution of bacterial ether lipids. Similarly, it is unclear whether pH plays an important factor. Some environments, such as marine sediments dominated by the process of anaerobic oxidation of methane where bacterial ether lipids are abundantly found, are more alkaline than their surrounding environment. However, the sediments and stratified water columns in these studies are relatively circumneutral. We therefore explore whether apart from temperature or pH, other variables, such as redox may influence backbone-chain linkage.

3.4.2. Number of Aliphatic Carbons, nC

As shown in Figures 6A,B, nC of alkyl chains tends to be greatest at the highest measured temperatures (above 80°C) and lowest dissolved oxygen concentration (around -5.0 log molal O_2). Values of nC approach 20 aliphatic carbons in samples furthest upstream, partly because these samples are rich in GDGTs with four 20-carbon half-chains. However, values of average nC approach 20 aliphatic carbons in upstream samples even after excluding contributions from GDGTs (empty symbols,



Figures 6A,B). Sample MS1 represents the only upstream sample where the weighted nC non-GDGT alkyl chains is anomalously small at 17.4 carbons, though it should be noted that non-GDGT chains comprise <1% of alkyl chains in this sample. Sample OS1 has the greatest weighted nC at 20.42 carbons because it was rich in C₅₀ and C₅₅ 2G-P-AR lipids that averaged 25 or 27.5 carbons per chain. Alkyl chain nC decreased with progressively cooler temperatures and oxidized conditions, reaching about 16.7–17 aliphatic carbons in samples furthest downstream. Overall, these trends in weighted nC agree with a plethora of studies demonstrating the capacity of microorganisms to adapt their membrane fluidity and permeability in response to temperature by adjusting the strength of hydrophobic interactions in the non-polar portion of their membranes (see reviews by Denich et al., 2003; van Meer et al., 2008; Siliakus et al., 2017).

3.4.3. Degree of Unsaturation, nUnsat

Average degree of unsaturation in IPL alkyl chains increased downstream in all four outflow channels, as shown in **Figures 6C,D**. Samples above 50°C or below -4.0 log molal O₂ had values of weighted nUnsat between 0 and 0.4 unsaturations and increased to 0.4–1 unsaturations in samples further downstream. This trend is especially prominent at Mound Spring

and Empress Pool, where nUnsat is near-zero in MS1 and EP1 and gradually increases to about 0.7 and 1 unsaturation per chain in MS5 and EP5, respectively. Inverse correlations between temperature and average degree of unsaturation are well-documented in the literature (Marr and Ingraham, 1962; Siliakus et al., 2017). An unsaturation can either be in the *cis* and *trans* configuration; a *cis*-unsaturation is thought to increase membrane fluidity by introducing a “kink” in an alkyl chain that decreases chain packing and disrupts neighboring lipids in the membrane. Conversely, relatively straight *trans*-unsaturated fatty acids reduce membrane fluidity and have been correlated with microbial growth at higher temperatures and resistance to solvents and desiccation (Okuyama et al., 1990, 1991; Weber et al., 1994; Halverson and Firestone, 2000; Kiran et al., 2004, 2005). Determination of *cis* or *trans* configurations in unsaturated IPL alkyl chains was beyond the analytical scope of this study, though it should be emphasized that Z_C is not affected by isomerism.

3.4.4. Degree of GDGT Cyclization

The incorporation of one or more cycloalkyl rings into the alkyl chains of GDGTs (e.g., Structure 16) has been proposed to enhance lipid packing while increasing fluidity in archaeal

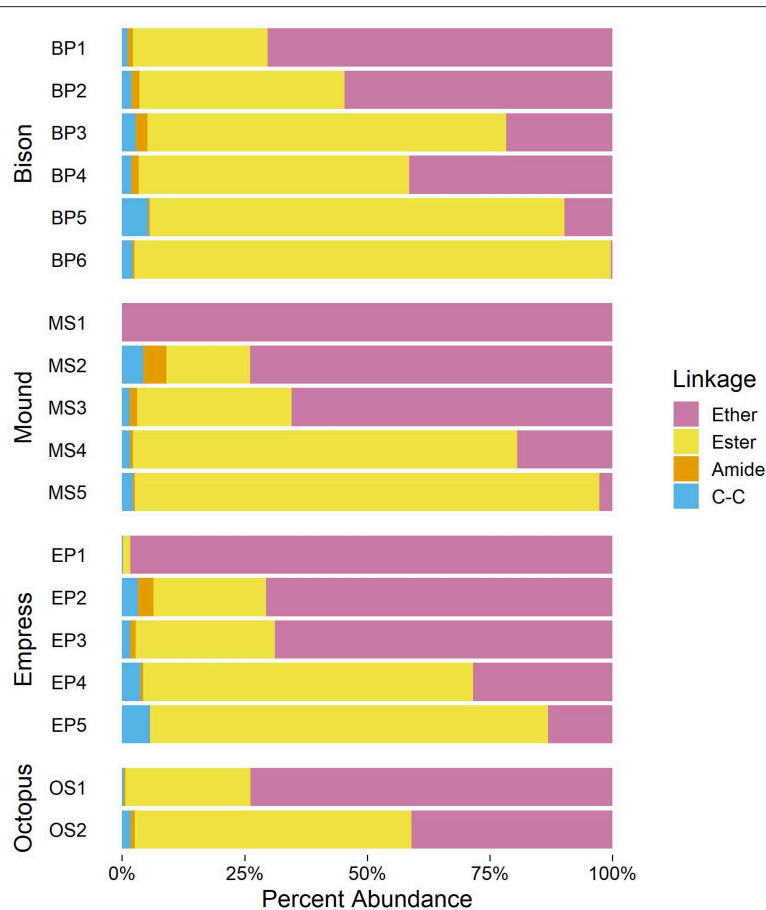


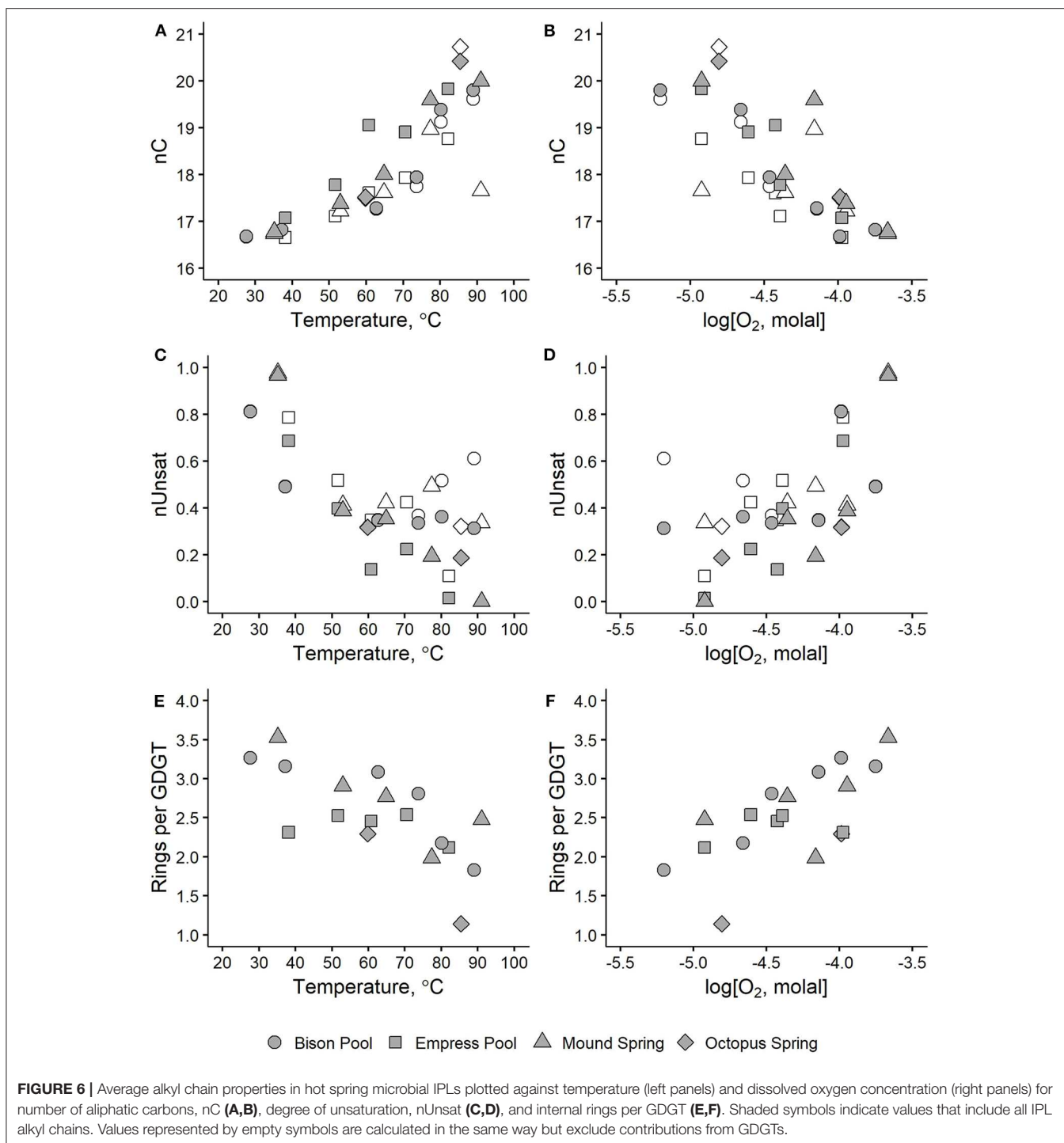
FIGURE 5 | Relative abundances of major backbone-alkyl chain linkage types in samples.

membranes (Gliozzi et al., 1983; Gabriel and Chong, 2000; Chong et al., 2012; Sollich et al., 2017). We observed a downstream increase in the number of internal rings in the GDGTs in the outflow channels of Bison Pool, Mound Spring, and Octopus Spring, as shown in **Figures 6E,F**. Between samples collected closest to each hot spring source and those furthest downstream, the average number of rings in GDGTs increased from 1.8 to 3.3 between BP1 and BP6, 2.5 to 3.5 between MS1 and MS5, and 1.1 to 2.5 between OS1 and OS2. Samples collected from the outflow channel of Empress Pool averaged between 2.1 and 2.5 rings and showed no clear correlation with temperature or dissolved oxygen concentration.

This downstream increase in the number of rings per GDGT agrees with a previous study by Schubotz et al. (2013) reporting a similar trend along the Bison Pool outflow channel. However, these results do not corroborate with studies by Schouten et al. (2002, 2007a) that propose a positive correlation between GDGT chain cyclization and temperature as the basis for the TEX_{86} paleothermometer (though TEX_{86} was originally calibrated for sea surface temperatures). Additionally, these observations do not match the results of laboratory growth experiments demonstrating increased chain cyclization with temperature

in thermoacidophilic archaea (Boyd et al., 2011), marine *Crenarchaeota* (Wuchter et al., 2004), and *Thaumarchaeota* (Elling et al., 2015). Conflicting trends have also been reported in terrestrial hydrothermal systems. Kaur et al. (2015) observed an increase in GDGT ring abundance with temperature between a pH range of 5.5–7.2 in hot springs from the Taupo volcanic zone in New Zealand, though their low pH samples did not. Wu et al. (2013) studied GDGTs in Yunnan hot springs, China, and found that ring index increased with temperature in one statistical grouping and increased with acidity in the other.

Low pH has been observed to cause an increase in GDGT chain cyclization (Macalady et al., 2004; Boyd et al., 2013), which has been attributed to a denser packing of the cell membrane resulting in a higher tolerance toward large ion gradients (Gabriel and Chong, 2000). Studies on the influence of high pH on the incorporation of the number of rings, comparable to our systems, have not been systematically conducted, therefore it remains unclear whether the change in pH from alkaline to circumneutral plays an important role in the downstream increase in the number of rings. However, we find it conversely conceivable that the lower pH conditions upstream may cause the incorporation of more rings for a denser packing of the membrane, which is



not reflected in our data. Temperature and pH have been cited as competing variables in numerous studies of GDGT ring index in hydrothermal systems and thermophilic archaea (Pearson et al., 2008; Boyd et al., 2011, 2013). It is still unclear how combinations of geochemical variables influence the incorporation of rings into archaeal membranes in a predictable way, though we propose that environmental redox conditions may influence ring distributions in section 3.6.

3.4.5. Number of Hydroxylations, nOH

Alkyl chains bearing a secondary hydroxyl group (e.g., Structure 20) comprised only a small portion (<1%) of total chains in our sample set (see Table S2). Even if the backbone hydroxylation of CER (9) and FA-OH-FAm-OH (11) are counted toward chain nOH, the total proportion of hydroxylated chains would only increase to a maximum of 4% in any sample.

3.5. Z_C of IPLs and Their Components

Downstream changes in IPLs and their component parts are reflected in their average chemical formulae (Table S3) and consequently, their Z_C values (Table S4). Trends in the Z_C of full IPLs and their headgroups, backbones, and alkyl chains are described below.

3.5.1. Full IPLs

Abundance-weighted Z_C values calculated for microbial IPLs collected from Bison Pool, Mound Spring, Empress Pool, and Octopus Spring are plotted against temperature and dissolved oxygen concentrations in Figure 7. It can be seen that decreasing temperature and increasingly oxidized conditions coincide with near-linear changes in the Z_C of IPLs. Carbon was most reduced in IPLs sampled closest to each hot spring source (Z_C between -1.68 and -1.56 in samples BP1, MS1, EP1, and OS1) where temperatures were highest (82.2 – 91.0°C) and oxidized inorganic species (nitrate, sulfate, and oxygen) had the lowest concentrations. In progressively downstream samples, carbon in IPLs became more oxidized, with Z_C between -1.36 and -1.33 for samples in between 29.0 and 38.1°C where measured concentrations of sulfate, nitrate, and oxygen tended to be highest.

Downstream trends remain intact after performing a statistical simulation of potential sources of analytical error,

as shown in Figure 7 by the black bars above and below the calculated values of Z_C . These bars indicate the standard deviation of Z_C values resulting from 999 iterations of the bootstrap sensitivity analysis. The standard deviations of IPL Z_C show little overlap between upstream and downstream samples after random variation of up to 30% for integrated HPLC-MS peak areas and up to two orders of magnitude for response factors.

3.5.2. Headgroups

Z_C values of IPL headgroups were most positive in mid-stream samples and most negative in samples furthest upstream and downstream (Figure 7). Upstream samples had relatively reduced headgroup carbon due to an abundance of 1G-GDGT lipids. These lipids have two headgroups according to our structural division scheme; a hexose and a hydrogen atom (e.g., the GDGT in Figure S9). This “hydrogen-only” headgroup drives down the Z_C of headgroups in upstream samples where 1G-GDGT is abundant. In downstream samples, phospholipids and aminolipids with relatively reduced headgroup carbon, such as PC, PE, PG, and TM-OL became more abundant and drove down the Z_C .

Glycolipid headgroups 1G ($Z_C = -0.16\bar{6}$) and 2G ($Z_C = -0.08\bar{3}$) were among the most abundant headgroups observed in all four springs regardless of temperature or redox state,

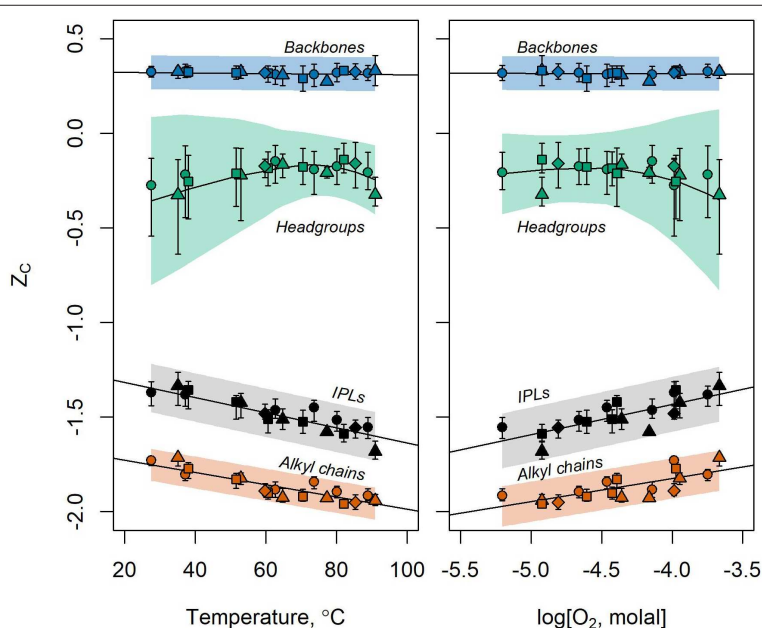


FIGURE 7 | Z_C of IPLs (black) and their headgroups (green), backbones (blue), alkyl chains (orange) sampled along the outflow channels of Bison Pool (circles), Mound Spring (triangles), Empress Pool (squares), and Octopus Spring (diamonds) with respect to temperature (left) and log molality of dissolved O_2 (right). Symbols designate the observed values of Z_C of extracted lipids and their components. Bars around the points show the standard deviation of 999 Z_C values resulting from the random variation of analytical peak areas and response factors during the bootstrap sensitivity analysis. Regression of these bootstrap values are indicated by fitted lines. Full lipids, backbones, and alkyl chains are fitted with linear regressions while headgroups are fit by local polynomial regression (LOESS). Shaded areas represent 95% prediction intervals for values of Z_C produced by the sensitivity analysis. LOESS regression was performed in R using the `loess.sd` function (“msir” package version 1.3.2) with parameters `nsigma = 1.96` (for the 95% prediction interval) and `span = 0.9` (for smoothing).

though they were most abundant, along with the glycolipid SQ ($Z_C = -0.166$) in samples where photosynthetic microorganisms are visually apparent. This agrees with observations that 1G, 2G, and SQ glycolipids are abundant in cyanobacterial (Wada and Murata, 2009) and algal (Guschina and Harwood, 2006) photosynthetic membranes.

Phosphate-bearing phospholipids and glycophospholipids, especially with PI headgroups, were more abundant downstream than upstream. However, the incorporation of phosphate itself into headgroups has no effect on abundance-weighted headgroup Z_C , as there is no difference in Z_C between analogous non-phosphorylated and phosphorylated headgroups (e.g., between 1G-P and 1G, or between 2G-P and 2G, *etc.*). The greatest abundance of lipids with an APT phospholipid headgroup ($Z_C = -0.6$) was observed in “pink streamer” thermophile communities sampled from the upstream chemosynthetic zones of Bison Pool and Octopus Spring; this result agrees with previous reports that this lipid is common in streamers with *Aquificales* bacteria (Sturt et al., 2004; Schubotz et al., 2013). However, after applying response factors, the abundance APT was low relative to other headgroups, even in streamer samples.

Values of Z_C for headgroups were substantially more sensitive to simulated sources of analytical uncertainty than those calculated for alkyl chains, backbones, or full IPLs. After 999 iterations of randomly adjusting response factors and HPLC-MS peak areas, the standard deviations in Z_C values (vertical bars in **Figure 7**) and the 95% prediction interval for future bootstrap calculations (shaded region) were greatest in magnitude for headgroups and overlapped for most samples. This calls into question the significance of downstream trends in headgroup Z_C , as they may be mere artifacts of the analytical method we used to quantify lipids.

3.5.3. Backbones

Backbones had the most oxidized carbon of any component owing to a high ratio of electronegative atoms (e.g., oxygen, nitrogen) to carbon. The Z_C of IPL backbones did not change significantly with temperature or redox state, as most observed backbones were composed of glycerol regardless of the sample location. A fully-linked glycerol backbone has a chemical formula of $C_3H_5O_3$ that corresponds to a Z_C of $0.33\bar{3}$. This is close to the average value in every sample, with little variation.

3.5.4. Alkyl Chains

Alkyl chains tend to have Z_C values ~ 0.3 – 0.4 more negative than those of the full structure regardless of the sample. The Z_C values of alkyl chains were closest to those of the full lipid compared to either headgroups or backbones, indicating that alkyl chains are the main contributor to the oxidation state of carbon in full lipids. This is unsurprising, given that alkyl chains generally contain more carbon than any other IPL component. Since alkyl chains have a high hydrogen:carbon ratio to facilitate their hydrophobicity, the weighted Z_C of IPLs and their chains are significantly more

negative than those of headgroups or backbones. Because alkyl chains contribute more to the average oxidation state of carbon in the full lipid than any other component, changes in alkyl chains are most responsible for the correlations observed between Z_C and temperature or dissolved oxygen in these hot spring outflow channels. Alkyl chain modifications with the most influence on Z_C were backbone-alkyl chain linkage chemistry, nC , $nUnsat$, and the number of internal rings per GDGT.

Changes in chain-backbone linkage chemistry correspond to a downstream increase in the Z_C of microbial IPLs stemming from the difference in chemical formulae between an ester and an ether bond. Carbon is more oxidized in an ester bond relative to an ether because it contains two fewer hydrogens and one more oxygen atom (compare Structures **13** and **18**). The number of aliphatic carbons in alkyl chains also has a great effect on Z_C . Each additional methylene group increases the chemical formula of a lipid by CH_2 for saturated chains, or by C_2H_4 for each methyl branch. Both of these groups have Z_C equal to -2 , so as more aliphatic carbons are added, the Z_C of an alkyl chain is driven closer to this value. This effect can be seen in **Figure 7**, where the Z_C of alkyl chains approach -2 in upstream samples where average nC is highest. Unsaturated alkyl chains are more oxidized than their saturated counterparts. This is because an alkyl chain with a double bond has two fewer hydrogen atoms (e.g., compare Structures **19** and **18**). This is also true for a GDGT ring (e.g., compare Structures **15** and **16**). As such, increased degree of unsaturation and GDGT ring indices contributed to the downstream increase in Z_C for lipids and their alkyl chains. Other alkyl chain modifications did not notably impact Z_C , either because they were observed at very low abundance, such as chain hydroxylations, or did not substantially change lipid chemical formulae, such as the single hydrogen difference between GDGT half-chains and the isoprenoidal chains of non-GDGTs (e.g., Structure **15** compared to **14**).

As shown in **Figure 7**, trends involving Z_C are more resistant to simulated sources of analytical uncertainty in alkyl chains than in full lipids. Linear regression of Z_C values produced by the bootstrap sensitivity analysis results in a narrower 95% prediction interval band for alkyl chains than for full lipids. Further, the standard deviations for individual samples tend to have narrower ranges, and overlap less, in alkyl chains. Taken together, we interpret this as evidence that the downstream increase in the Z_C of alkyl chains is not an artifact of the analytical method used to quantify lipid abundance.

3.6. Redox and Lipid Composition

Thermodynamic analyses are needed to test how redox constraints influence the energetic favorability of lipid modifications, such as alkyl chain length, degree of unsaturation, ester and ether alkyl chain linkage, headgroup type, and so on. Several experiments have already yielded intriguing evidence that the expression of ringed GDGT alkyl chains is favorable under oxidized conditions. Following a laboratory study by Qin et al. (2015) that implicated O_2 limitation

as a confounding factor when interpreting TEX_{86} -derived temperatures, Hurley et al. (2016) showed an inverse correlation between ammonia oxidation rate and degree of ring cyclization in GDGTs of cultured ammonia oxidizing *Thaumarchaeota* and hypothesized that the supply of NH_4^+ , provides the reduction potential necessary to drive saturation to GDGT-0 during lipid synthesis. Further evidence was provided by (Evans et al., 2018), who showed that ammonia oxidizing *Nitrosopumilus maritimus* produces GDGTs with fewer rings when grown in media containing excess NH_4^+ . Zhou et al. (2019) found that GDGT cyclization from electron supply limitation also occurred in thermoacidophilic *Sulfolobus acidocaldarius* cultures. If sufficient reduction potential is necessary to saturate GDGTs, then an increasingly limited electron supply from ammonia, sulfide, and/or other electron donors may be responsible for the downstream increase in the average number of rings per GDGT found in Bison Pool, Mound Spring, and Octopus Spring. This may also explain why fewer GDGT rings were observed downstream in this study and in Schubotz et al. (2013), which is seemingly at odds with temperature-derived trends reported in various culture experiments (Wuchter et al., 2004; Boyd et al., 2011; Elling et al., 2015) and used in the TEX_{86} paleothermometer (Schouten et al., 2002, 2007a), though redox conditions were not the focus of these studies.

It is intriguing to consider that other lipid structural modifications, or even entire lipid compositions, may be sensitive to redox constraints. Lipid compositions produced by a microbial community might tend to be “electron-rich” (low Z_C) under reduced environmental conditions where electron supply is high, and “electron-poor” (high Z_C) under oxidized conditions where electron supply is low. If such a compositional advantage exists, then trends in lipid Z_C may be evident along other environmental redox gradients. For instance, studies of IPL distributions in the Black Sea have reported changes in alkyl chain structure along relatively isothermal redox gradients similar to those found along the hot spring outflow channels in this study; deeper sampling in the water column coincides with a pronounced shift in ester- to ether- linked alkyl chains, an increase in nC, a decrease in nUnsat, and an increase in the abundance of GDGTs and ARs (Schubotz et al., 2009; Schröder, 2015; Evans et al., 2017). Based on our approach, IPLs in the oxic zone of the Black Sea have relatively oxidized carbon, while deeper and more reduced conditions correspond to increasingly reduced carbon. This fits the general pattern observed in this study, and may indicate a biological drive for microbial communities to synthesize stable membranes within the redox constraints of their surroundings. If so, Z_C information preserved in lipid biomarker compositions could offer valuable insights into the geochemical paleoredox conditions experienced by source organisms. These hypotheses can be tested in a variety of natural systems by comparing the Z_C of IPLs produced by the microbial communities to concurrent redox measurements. Studies that strive for completeness and quantitative accuracy in their underlying lipid and geochemical datasets will be extraordinarily valuable for investigating these potential relationships.

4. CONCLUDING REMARKS

Lipids were extracted from microbial communities sampled spatially along the outflow channels of four alkaline hot springs in Yellowstone National Park. Chemical formulae and relative abundances of lipid structures interpreted from HPLC-MS/MS were used to calculate the average oxidation state of carbon, Z_C , for lipids in each sample. Values of Z_C were also calculated for lipid headgroups, backbones, and alkyl chains. We found that lipids extracted from microbial communities living under the hottest, most reduced conditions had the most reduced carbon (lowest Z_C). This is because lipids in upstream samples contained a greater number of modifications that increased their hydrogen-to-carbon ratio, including alkyl chains with a greater number of aliphatic carbons, fewer unsaturations, fewer GDGT rings, and linked to the backbone with a higher proportion of ether bonds. The Z_C of lipids increased (representing increasingly more oxidized carbon) with distance downstream, coinciding with more oxidized conditions and cooler temperatures. Lipids sampled furthest downstream had the most oxidized carbon (highest Z_C) resulting from an abundance of alkyl chain modifications that decreased their hydrogen-to-carbon ratio (fewer aliphatic carbons, higher degree of unsaturation, a greater number of GDGT rings, and a greater proportion of ester-linkage). These alkyl chain modifications permit membrane function in the microbial communities sampled across the extreme temperature gradients of Yellowstone outflow channels. The tendency to find oxidized lipid modifications under oxidized conditions and vice versa for reduced conditions may represent adaptation to limitations in available reduction potential imposed by concentrations of electron donors and acceptors in the surrounding water. If this pattern is widespread, the Z_C of bulk lipid compositions could become a useful metric for assessing prevailing redox across a variety of natural settings. Preserved in lipid biomarkers, these Z_C signatures could offer a window into redox conditions of the past.

DATA AVAILABILITY STATEMENT

The code and IPL abundance data used in this study can be found in the repository PolarLipidZC, <https://gitlab.com/gmboyer/polarlipidzc>.

AUTHOR CONTRIBUTIONS

GB and ES conceived the study. GB and JW performed the lipid extractions. GB and FS analyzed the HPLC-MS data. GB performed the calculations. All authors contributed to the writing and revision of this manuscript.

FUNDING

Research reported here was funded by NSF grants EAR-1123649 and EAR-1529963, and NASA Exobiology grant NNX16AJ61G. FS acknowledges funding from the Alexander von Humboldt society and the Central Research Development Fund of the University of Bremen. Financial support for

the lipid analyses conducted at MIT was provided by the NASA Astrobiology Institute NNA13AA90A, Foundations of Complex Life, Evolution, Preservation, and Detection on Earth and Beyond.

ACKNOWLEDGMENTS

We thank Kris Fecteau, Kirt Robinson, Brian St. Clair, Vince Debes, Kristin Johnson, Apar Prasad, and Alta Howells for their

help in collecting and analyzing water geochemistry data. We also thank Jeff Dick for valuable discussions regarding the Z_C of biomolecules.

SUPPLEMENTARY MATERIAL

The Supplementary Material for this article can be found online at: <https://www.frontiersin.org/articles/10.3389/fmicb.2020.00229/full#supplementary-material>

REFERENCES

- Adams, B. L., McMahon, V., and Seckbach, J. (1971). Fatty acids in the thermophilic alga, *Cyanidium caldarium*. *Biochem. Biophys. Res. Commun.* 42, 359–365.
- Amend, J. P., and Shock, E. L. (1998). Energetics of amino acid synthesis in hydrothermal ecosystems. *Science* 281, 1659–1662.
- Barns, S. M., Delwiche, C. F., Palmer, J. D., and Pace, N. R. (1996). Perspectives on archaeal diversity, thermophily and monophyly from environmental rRNA sequences. *Proc. Natl. Acad. Sci. U.S.A.* 93, 9188–9193.
- Barns, S. M., Fundyga, R. E., Jeffries, M. W., and Pace, N. R. (1994). Remarkable archaeal diversity detected in a Yellowstone National Park hot spring environment. *Proc. Natl. Acad. Sci. U.S.A.* 91, 1609–1613.
- Beam, J. P., Jay, Z. J., Schmid, M. C., Rusch, D. B., Romine, M. F., Jennings, R. M., et al. (2016). Ecophysiology of an uncultivated lineage of *Aigarchaeota* from anoxic, hot spring filamentous “streamer” community. *ISME J.* 10, 210–224. doi: 10.1038/ismej.2015.83
- Benning, C., Huang, Z.-H., and Gage, D. A. (1995). Accumulation of a novel glycolipid and a betaine lipid in cells of *Rhodobacter sphaeroides* grown under phosphate limitation. *Arch. Biochem. Biophys.* 317, 103–111.
- Boyd, E., Hamilton, T., Wang, J., He, L., and Zhang, C. (2013). The role of tetraether lipid composition in the adaptation of thermophilic archaea to acidity. *Front. Microbiol.* 4:62. doi: 10.3389/fmicb.2013.00062
- Boyd, E. S., Pearson, A., Pi, Y., Li, W.-J., Zhang, Y. G., He, L., et al. (2011). Temperature and pH controls on glycerol dibiphytanyl glycerol tetraether lipid composition in the hyperthermophilic crenarchaeon *Acidilobus sulfurireducens*. *Extremophiles* 15, 59–65. doi: 10.1007/s00792-010-0339-y
- Boye, K., Noël, V., Tfaily, M. M., Bone, S. E., Williams, K. H., Bargar, J. R., et al. (2017). Thermodynamically controlled preservation of organic carbon in floodplains. *Nat. Geosci.* 10:415. doi: 10.1038/ngeo2940
- Brocks, J. J., and Pearson, A. (2005). Building the biomarker tree of life. *Rev. Mineral. Geochem.* 59, 233–258. doi: 10.2138/rmg.2005.59.10
- Chong, P. L. G., Ayesa, U., Prakash Daswani, V., and Hur, E. C. (2012). On physical properties of tetraether lipid membranes: effects of cyclopentane rings. *Archaea* 2012:12. doi: 10.1155/2012/138439
- Colman, D. R., Jay, Z. J., Inskeep, W. P., Jennings, R. M., Maas, K. R., Rusch, D. B., et al. (2016). Novel, deep-branching heterotrophic bacterial populations recovered from thermal spring metagenomes. *Front. Microbiol.* 7:304. doi: 10.3389/fmicb.2016.00304
- Cox, A., Shock, E. L., and Havig, J. R. (2011). The transition to microbial photosynthesis in hot spring ecosystems. *Chem. Geol.* 280, 344–351. doi: 10.1016/j.chemgeo.2010.11.022
- Curatolo, W. (1987). Glycolipid function. *Biochim. Biophys. Acta* 906, 137–160.
- Daniel, R. M., and Cowan, D. A. (2000). Biomolecular stability and life at high temperatures. *Cell. Mol. Life Sci.* 57, 250–264. doi: 10.1007/PL00000688
- Denich, T. J., Beaudette, L. A., Lee, H., and Trevors, J. T. (2003). Effect of selected environmental and physico-chemical factors on bacterial cytoplasmic membranes. *J. Microbiol. Methods* 52, 149–182. doi: 10.1016/S0167-7012(02)00155-0
- Dick, J. M. (2014). Average oxidation state of carbon in proteins. *J. R. Soc. Interface* 11:20131095. doi: 10.1098/rsif.2013.1095
- Dick, J. M. (2016). Proteomic indicators of oxidation and hydration state in colorectal cancer. *PeerJ* 4:e2238. doi: 10.7717/peerj.2238
- Dick, J. M. (2017). Chemical composition and the potential for proteomic transformation in cancer, hypoxia, and hyperosmotic stress. *PeerJ* 5:e3421. doi: 10.7717/peerj.3421
- Dick, J. M., and Shock, E. L. (2011). Calculation of the relative chemical stabilities of proteins as a function of temperature and redox chemistry in a hot spring. *Public Lib. Sci. One* 6:e22782. doi: 10.1371/journal.pone.0022782
- Dick, J. M., and Shock, E. L. (2013). A metastable equilibrium model for the relative abundances of microbial phyla in a hot spring. *Public Lib. Sci. One* 8:e72395. doi: 10.1371/journal.pone.0072395
- Dick, J. M., Yu, M., Tan, J., and Lu, A. (2019). Changes in carbon oxidation state of metagenomes along geochemical redox gradients. *Front. Microbiol.* 10:120. doi: 10.3389/fmicb.2019.00120
- Diercks, H., Semeniuk, A., Gisch, N., Moll, H., Duda, K. A., and Hölzl, G. (2015). Accumulation of novel glycolipids and ornithine lipids in *Mesorhizobium loti* under phosphate deprivation. *J. Bacteriol.* 197, 497–509. doi: 10.1128/JB.02004-14
- Dupraz, C., and Visscher, P. T. (2005). Microbial lithification in marine stromatolites and hypersaline mats. *Trends Microbiol.* 13, 429–438. doi: 10.1016/j.tim.2005.07.008
- Elling, F. J., Könneke, M., Mußmann, M., Greve, A., and Hinrichs, K.-U. (2015). Influence of temperature, pH, and salinity on membrane lipid composition and TEX₈₆ of marine planktonic thaumarchaeal isolates. *Geochim. Cosmochim. Acta* 171, 238–255. doi: 10.1016/j.gca.2015.09.004
- Evans, T. W., Könneke, M., Lipp, J. S., Adhikari, R. R., Taubner, H., Elvert, M., et al. (2018). Lipid biosynthesis of *Nitrosopumilus maritimus* dissected by lipid specific radioisotope probing (lipid-RIP) under contrasting ammonium supply. *Geochim. Cosmochim. Acta* 242, 51–63. doi: 10.1016/j.gca.2018.09.001
- Evans, T. W., Wörmer, L., Lever, M. A., Lipp, J. S., Lagostina, L., Lin, Y.-S., et al. (2017). Size and composition of seafloor microbial community in the Benguela upwelling area examined from intact membrane lipid and DNA analysis. *Organ. Geochem.* 111, 86–100. doi: 10.1016/j.orggeochem.2017.06.008
- Fenchel, T. (1998). Artificial cyanobacterial mats: cycling of C, O, and S. *Aquat. Microb. Ecol.* 14, 253–259.
- Ferreira, A. M., Wait, R., Nobre, M. F., and da Costa, M. S. (1999). Characterization of glycolipids from *Meiothermus* spp. *Microbiology* 145, 1191–1199.
- Fones, E. M., Colman, D. R., Kraus, E. A., Nothaft, D. B., Poudel, S., Rempfert, K. R., et al. (2019). Physiological adaptations to serpentinization in the Samail Ophiolite, Oman. *ISME J.* 13, 1750–1762. doi: 10.1038/s41396-019-0391-2
- Franks, J., and Stolz, J. F. (2009). Flat laminated microbial mat communities. *Earth Sci. Rev.* 96, 163–172. doi: 10.1016/j.earscirev.2008.10.004
- French, K. L., Hallmann, C., Hope, J. M., Schoon, P. L., Zumbege, J. A., Hoshino, Y., et al. (2015). Reappraisal of hydrocarbon biomarkers in Archean rocks. *Proc. Natl. Acad. Sci. U.S.A.* 112, 5915–5920. doi: 10.1073/pnas.1419563112
- Gabriel, J. L., and Chong, P. L. G. (2000). Molecular modeling of archaeobacterial bipolar tetraether lipid membranes. *Chem. Phys. Lipids* 105, 193–200. doi: 10.1016/S0009-3084(00)00126-2
- Gliozzi, A., Paoli, G., De Rosa, M., and Gambacorta, A. (1983). Effect of isoprenoid cyclization on the transition temperature of lipids in thermophilic archaeobacteria. *Biochim. Biophys. Acta* 735, 234–242.
- Grogan, D. W., and Cronan, J. E. (1997). Cyclopropane ring formation in membrane lipids of bacteria. *Microbiol. Mol. Biol. Rev.* 61, 429–441.
- Guschina, I. A., and Harwood, J. L. (2006). Lipids and lipid metabolism in eukaryotic algae. *Prog. Lipid Res.* 45, 160–186. doi: 10.1016/j.plipres.2006.01.001

- Halverson, L. J., and Firestone, M. K. (2000). Differential effects of permeating and nonpermeating solutes on the fatty acid composition of *Pseudomonas putida*. *Appl. Environ. Microbiol.* 66, 2414–2421. doi: 10.1128/AEM.66.6.2414-2421.2000
- Huber, R., Wilharm, T., Huber, D., Trinconne, A., Burggraf, S., König, H., et al. (1992). *Aquifex pyrophilus* gen. nov. sp. nov., represents a novel group of marine hyperthermophilic hydrogen-oxidizing bacteria. *Syst. Appl. Microbiol.* 15, 340–351. doi: 10.1016/S0723-2020(11)80206-7
- Hurley, S. J., Elling, F. J., Könneke, M., Buchwald, C., Wankel, S. D., Santoro, A. E., et al. (2016). Influence of ammonia oxidation rate on thaumarchaeal lipid composition and the TEX₈₆ temperature proxy. *Proc. Natl. Acad. Sci. U.S.A.* 113, 7762–7767. doi: 10.1073/pnas.1518534113
- Jahnke, L. L., Eder, W., Huber, R., Hope, J. M., Hinrichs, K.-U., Hayes, J. M., et al. (2001). Signature lipids and stable carbon isotope analyses of Octopus Spring hyperthermophilic communities compared with those of *Aquificales* representatives. *Appl. Environ. Microbiol.* 67, 5179–5189. doi: 10.1128/AEM.67.11.5179-5189.2001
- Jonkers, H. M., Ludwig, R., De Wit, R., Pringault, O., Muyzer, G., Niemann, H., et al. (2003). Structural and functional analysis of a microbial mat ecosystem from a unique permanent hypersaline inland lake: “La Salada de Chiprana” (NE Spain). *FEMS Microbiol. Ecol.* 44, 175–189. doi: 10.1016/S0168-6496(02)00464-6
- Karlsson, A. Å., Michélsen, P., and Odham, G. (1998). Molecular species of sphingomyelin: determination by high-performance liquid chromatography/mass spectrometry with electrospray and high-performance liquid chromatography/tandem mass spectrometry with atmospheric pressure chemical ionization. *J. Mass Spectr.* 33, 1192–1198.
- Kaur, G., Mountain, B. W., Stott, M. B., Hopmans, E. C., and Pancost, R. D. (2015). Temperature and pH control on lipid composition of silica sinters from diverse hot springs in the Taupo Volcanic Zone, New Zealand. *Extremophiles* 19, 327–344. doi: 10.1007/s00792-014-0719-9
- Kent, C. (1995). Eukaryotic phospholipid biosynthesis. *Annu. Rev. Biochem.* 64, 315–343.
- Kiran, M., Prakash, J., Annapoorni, S., Dube, S., Kusano, T., Okuyama, H., et al. (2004). Psychrophilic *Pseudomonas syringae* requires *trans*-monounsaturated fatty acid for growth at higher temperature. *Extremophiles* 8, 401–410. doi: 10.1007/s00792-004-0401-8
- Kiran, M. D., Annapoorni, S., Suzuki, I., Murata, N., and Shivaji, S. (2005). *Cis-trans* isomerase gene in psychrophilic *Pseudomonas syringae* is constitutively expressed during growth and under conditions of temperature and solvent stress. *Extremophiles* 9, 117–125. doi: 10.1007/s00792-005-0435-6
- Kroll, J. H., Donahue, N. M., Jimenez, J. L., Kessler, S. H., Canagaratna, M. R., Wilson, K. R., et al. (2011). Carbon oxidation state as a metric for describing the chemistry of atmospheric organic aerosol. *Nat. Chem.* 3:133. doi: 10.1038/nchem.948
- Kroll, J. H., Lim, C. Y., Kessler, S. H., and Wilson, K. R. (2015). Heterogeneous oxidation of atmospheric organic aerosol: kinetics of changes to the amount and oxidation state of particle-phase organic carbon. *J. Phys. Chem. A* 119, 10767–10783. doi: 10.1021/acs.jpca.5b06946
- LaRowe, D. E., and Van Cappellen, P. (2011). Degradation of natural organic matter: a thermodynamic analysis. *Geochim. Cosmochim. Acta* 75, 2030–2042. doi: 10.1016/j.gca.2011.01.020
- Likens, G. E. (Eds.). (2010). *Biogeochemistry of Inland Waters*. Millbrook, NY: Academic Press.
- Loiacono, S. T. (2013). *Merging genomics, transcriptomics and geochemistry to assess nitrogen cycling in terrestrial hot springs* (MS thesis). University of Illinois at Chicago, Chicago, IL, United States.
- López-Lara, I. M., and Geiger, O. (2017). Bacterial lipid diversity. *Biochim. Biophys. Acta* 1862, 1287–1299. doi: 10.1016/j.bbali.2016.10.007
- Macalady, J. L., Vestling, M. M., Baumler, D., Boekelheide, N., Kaspar, C. W., and Banfield, J. F. (2004). Tetraether-linked membrane monolayers in *Ferroplasma* spp: a key to survival in acid. *Extremophiles* 8, 411–419. doi: 10.1007/s00792-004-0404-5
- Marr, A. G., and Ingraham, J. L. (1962). Effect of temperature on the composition of fatty acids in *Escherichia coli*. *J. Bacteriol.* 84, 1260–1267.
- Meyer-Dombard, D. R., Shock, E. L., and Amend, J. P. (2005). Archaeal and bacterial communities in geochemically diverse hot springs of Yellowstone National Park, USA. *Geobiology* 3, 211–227. doi: 10.1111/j.1472-4669.2005.00052.x
- Meyer-Dombard, D. R., Swingley, W., Raymond, J., Havig, J., Shock, E. L., and Summons, R. E. (2011). Hydrothermal ecotones and streamer biofilm communities in the Lower Geyser Basin, Yellowstone National Park. *Environ. Microbiol.* 13, 2216–2231. doi: 10.1111/j.1462-2920.2011.02476.x
- Moore, E. K., Hopmans, E. C., Rijpstra, W. I. C., Villanueva, L., Dedysh, S. N., Kulichevskaya, I. S., et al. (2013). Novel mono-, di-, and trimethylornithine membrane lipids in northern wetland planctomycetes. *Appl. Environ. Microbiol.* 79, 6874–6884. doi: 10.1128/AEM.02169-13
- Murata, N., and Siegenthaler, P.-A. (eds.). (1998). “Lipids in photosynthesis: an overview,” in *Lipids in Photosynthesis: Structure, Function and Genetics* (Dordrecht: Kluwer Academic Publishers), 1–20.
- Nishihara, M., and Koga, Y. (1987). Extraction and composition of polar lipids from the archaeobacterium, *Methanobacterium thermoautotrophicum*: effective extraction of tetraether lipids by an acidified solvent. *J. Biochem.* 101, 997–1005.
- Okuyama, H., Okajima, N., Sasaki, S., Higashi, S., and Murata, N. (1991). The *cis/trans* isomerization of the double bond of a fatty acid as a strategy for adaptation to changes in ambient temperature in the psychrophilic bacterium, *Vibrio* sp. strain ABE-1. *Biochim. Biophys. Acta* 1084, 13–20.
- Okuyama, H., Sasaki, S., Higashi, S., and Murata, N. (1990). A *trans*-unsaturated fatty acid in a psychrophilic bacterium, *Vibrio* sp. strain ABE-1. *J. Bacteriol.* 172, 3515–3518.
- Pearson, A., and Ingalls, A. E. (2013). Assessing the use of archaeal lipids as marine environmental proxies. *Annu. Rev. Earth Planet. Sci.* 41, 359–384. doi: 10.1146/annurev-earth-050212-123947
- Pearson, A., Pi, Y., Zhao, W., Li, W., Li, Y., Inskeep, W., et al. (2008). Factors controlling the distribution of archaeal tetraethers in terrestrial hot springs. *Appl. Environ. Microbiol.* 74, 3523–3532. doi: 10.1128/AEM.02450-07
- Pitcher, A., Schouten, S., and Damsté, J. S. S. (2009). In situ production of crenarchaeol in two California hot springs. *Appl. Environ. Microbiol.* 75, 4443–4451. doi: 10.1128/AEM.02591-08
- Popendorf, K. J., Fredricks, H. F., and Van Mooy, B. A. (2013). Molecular ion-independent quantification of polar glycerolipid classes in marine plankton using triple quadrupole MS. *Lipids* 48, 185–195. doi: 10.1007/s11745-012-3748-0
- Poudel, S., Colman, D. R., Fixen, K. R., Ledbetter, R. N., Zheng, Y., Pence, N., et al. (2018). Electron transfer to nitrogenase in different genomic and metabolic backgrounds. *J. Bacteriol.* 200:e00757-17. doi: 10.1128/JB.00757-17
- Prado, A., Da Costa, M. S., and Madeira, V. M. (1988). Effect of growth temperature on the lipid composition of two strains of *Thermus* sp. *Microbiology* 134, 1653–1660.
- Qin, W., Carlson, L. T., Armbrust, E. V., Devol, A. H., Moffett, J. W., Stahl, D. A., et al. (2015). Confounding effects of oxygen and temperature on the TEX₈₆ signature of marine thaumarchaeota. *Proc. Natl. Acad. Sci. U.S.A.* 112, 10979–10984. doi: 10.1073/pnas.1501568112
- Rashby, S. E., Sessions, A. L., Summons, R. E., and Newman, D. K. (2007). Biosynthesis of 2-methylbacteriohopanepolyols by an anoxygenic phototroph. *Proc. Natl. Acad. Sci. U.S.A.* 104, 15099–15104. doi: 10.1073/pnas.0704912104
- Ray, P. H., White, D. C., and Brock, T. D. (1971). Effect of growth temperature on the lipid composition of *Thermus aquaticus*. *J. Bacteriol.* 108, 227–235.
- Reysenbach, A.-L., Wickham, G. S., and Pace, N. R. (1994). Phylogenetic analysis of the hyperthermophilic pink filament community in Octopus Spring, Yellowstone National Park. *Appl. Environ. Microbiol.* 60, 2113–2119.
- Romero, J. T. (2018). *Changes in microbial communities and geochemical energy supplies across the photosynthetic fringe of hot spring outflows in Yellowstone National Park* (MS thesis). Arizona State University Tempe, AZ, United States.
- Sato, N. (2004). Roles of the acidic lipids sulfoquinovosyl diacylglycerol and phosphatidylglycerol in photosynthesis: their specificity and evolution. *J. Plant Res.* 117, 495–505. doi: 10.1007/s10265-004-0183-1
- Schouten, S., Forster, A., Panoto, F. E., and Damsté, J. S. S. (2007a). Towards calibration of the TEX₈₆ palaeothermometer for tropical sea surface temperatures in ancient greenhouse worlds. *Organ. Geochem.* 38, 1537–1546. doi: 10.1016/j.orggeochem.2007.05.014
- Schouten, S., Hopmans, E. C., and Damsté, J. S. S. (2013). The organic geochemistry of glycerol dialkyl glycerol tetraether lipids: a review. *Organ. Geochem.* 54, 19–61. doi: 10.1016/j.orggeochem.2012.09.006

- Schouten, S., Hopmans, E. C., Schefuß, E., and Damste, J. S. S. (2002). Distributional variations in marine crenarchaeotal membrane lipids: a new tool for reconstructing ancient sea water temperatures? *Earth Planet. Sci. Lett.* 204, 265–274. doi: 10.1016/S0012-821X(02)00979-2
- Schouten, S., Meer, M., Hopmans, E., Rijpstra, W., Reysenbach, A., Ward, D., et al. (2007b). Archaeal and bacterial glycerol dialkyl glycerol tetraether lipids in hot springs of Yellowstone National Park. *Appl. Environ. Microbiol.* 73, 6181–6191. doi: 10.1128/AEM.00630-07
- Schröder, J. M. (2015). *Intact polar lipids in marine sediments: improving analytical protocols and assessing planktonic and benthic sources* (Dissertation). Staats- und Universitätsbibliothek Bremen, Bremen, Germany.
- Schubotz, F., Hays, L. E., Meyer-Dombard, D'R., Gillespie, A., Shock, E. L., and Summons, R. E. (2015). Stable isotope labeling confirms mixotrophic nature of streamer biofilm communities at alkaline hot springs. *Front. Microbiol.* 6:42. doi: 10.3389/fmicb.2015.00042
- Schubotz, F., Meyer-Dombard, D., Bradley, A., Fredricks, H., Hinrichs, K., Shock, E., et al. (2013). Spatial and temporal variability of biomarkers and microbial diversity reveal metabolic and community flexibility in Streamer Biofilm Communities in the Lower Geyser Basin, Yellowstone National Park. *Geobiology* 11, 549–569. doi: 10.1111/gbi.12051
- Schubotz, F., Wakeham, S. G., Lipp, J. S., Fredricks, H. F., and Hinrichs, K.-U. (2009). Detection of microbial biomass by intact polar membrane lipid analysis in the water column and surface sediments of the Black Sea. *Environ. Microbiol.* 11, 2720–2734. doi: 10.1111/j.1462-2920.2009.01999.x
- Siliakus, M. F., van der Oost, J., and Kengen, S. W. (2017). Adaptations of archaeal and bacterial membranes to variations in temperature, pH and pressure. *Extremophiles* 21, 651–670. doi: 10.1007/s00792-017-0939-x
- Sollich, M., Yoshinaga, M. Y., Häusler, S., Price, R. E., Hinrichs, K.-U., and Bühring, S. I. (2017). Heat stress dictates microbial lipid composition along a thermal gradient in marine sediments. *Front. Microbiol.* 8:1550. doi: 10.3389/fmicb.2017.01550
- Spear, J. R., Walker, J. J., McCollom, T. M., and Pace, N. R. (2005). Hydrogen and bioenergetics in the Yellowstone geothermal ecosystem. *Proc. Natl. Acad. Sci. U.S.A.* 102, 2555–2560. doi: 10.1073/pnas.0409574102
- Sturt, H. F., Summons, R. E., Smith, K., Elvert, M., and Hinrichs, K.-U. (2004). Intact polar membrane lipids in prokaryotes and sediments deciphered by high-performance liquid chromatography/electrospray ionization multistage mass spectrometry—new biomarkers for biogeochemistry and microbial ecology. *Rapid Commun. Mass Spectr.* 18, 617–628. doi: 10.1002/rcm.1378
- Summons, R. E., Jahnke, L. L., Hope, J. M., and Logan, G. A. (1999). 2-Methylhopanoids as biomarkers for cyanobacterial oxygenic photosynthesis. *Nature* 400:554.
- Summons, R. E., and Walter, M. R. (1990). Molecular fossils and microfossils of prokaryotes and protists from Proterozoic sediments. *Am. J. Sci.* 290, 212–244.
- Swingle, W. D., D'Arcy, R., Shock, E. L., Alsop, E. B., Falenski, H. D., Havig, J. R., et al. (2012). Coordinating environmental genomics and geochemistry reveals metabolic transitions in a hot spring ecosystem. *PLoS ONE* 7:e38108. doi: 10.1371/journal.pone.0038108
- Tansey, M. R., and Brock, T. D. (1972). The upper temperature limit for eukaryotic organisms. *Proc. Natl. Acad. Sci. U.S.A.* 69, 2426–2428.
- van Meer, G., Voelker, D. R., and Feigenson, G. W. (2008). Membrane lipids: where they are and how they behave. *Nat. Rev. Mol. Cell Biol.* 9:112. doi: 10.1038/nrm2330
- Vinçon-Laugier, A., Cravo-Laureau, C., Mitteau, I., and Grossi, V. (2017). Temperature-dependent alkyl glycerol ether lipid composition of mesophilic and thermophilic sulfate-reducing bacteria. *Front. Microbiol.* 8:1532. doi: 10.3389/fmicb.2017.01532
- Visser, P. T., Reid, R. P., Bebout, B. M., Hoefft, S. E., Macintyre, I. G., and Thompson, J. A. (1998). Formation of lithified micritic laminae in modern marine stromatolites (Bahamas): the role of sulfur cycling. *Am. Mineral.* 83, 1482–1493.
- Wada, H., and Murata, N. (2009). “Lipids in thylakoid membranes and photosynthetic cells,” in *Lipids in Photosynthesis*, eds H. Wada and N. Murata (Dordrecht: Springer), 1–9.
- Wang, M., Kim, G. H., Wei, F., Chen, H., Altarejos, J., and Han, X. (2015). Improved method for quantitative analysis of methylated phosphatidylethanolamine species and its application for analysis of diabetic-mouse liver samples. *Anal. Bioanal. Chem.* 407, 5021–5032. doi: 10.1007/s00216-015-8534-4
- Ward, D. M., Tayne, T. A., Anderson, K. L., and Bateson, M. M. (1987). “Community structure and interactions among community members in hot spring cyanobacterial mats,” in *Symposia of the Society for General Microbiology* (Cambridge).
- Weber, F. J., Isken, S., and De Bont, J. A. (1994). *Cis/trans* isomerization of fatty acids as a defence mechanism of *Pseudomonas putida* strains to toxic concentrations of toluene. *Microbiology* 140, 2013–2017.
- White, D. C., and Ringelberg, D. B. (1998). “Signature lipid biomarker analysis,” in *Techniques in Microbial Ecology*, Vol. 255, eds R. S. Burlage, R. Atlas, D. Stahl, G. Geesey, and G. Saylor (New York, NY: Oxford University Press), 255–272.
- Wörmer, L., Lipp, J. S., Schröder, J. M., and Hinrichs, K.-U. (2013). Application of two new LC-ESI-MS methods for improved detection of intact polar lipids (IPLs) in environmental samples. *Organ. Geochem.* 59, 10–21. doi: 10.1016/j.orggeochem.2013.03.004
- Wu, W., Zhang, C., Wang, H., He, L., Li, W., and Dong, H. (2013). Impacts of temperature and pH on the distribution of archaeal lipids in Yunnan hot springs, China. *Front. Microbiol.* 4:312. doi: 10.3389/fmicb.2013.00312
- Wuchter, C., Schouten, S., Coolen, M. J., and Sinninghe Damsté, J. S. (2004). Temperature-dependent variation in the distribution of tetraether membrane lipids of marine Crenarchaeota: implications for TEX₈₆ paleothermometry. *Paleoceanography* 19, 1–10. doi: 10.1029/2004PA001041
- Yang, Y.-L., Yang, F.-L., Jao, S.-C., Chen, M.-Y., Tsay, S.-S., Zou, W., et al. (2006). Structural elucidation of phosphoglycolipids from strains of the bacterial thermophiles *Thermus* and *Meiothermus*. *J. Lipid Res.* 47, 1823–1832. doi: 10.1194/jlr.M600034-JLR200
- Yoshinaga, M. Y., Kellermann, M. Y., Rossel, P. E., Schubotz, F., Lipp, J. S., and Hinrichs, K.-U. (2011). Systematic fragmentation patterns of archaeal intact polar lipids by high-performance liquid chromatography/electrospray ionization ion-trap mass spectrometry. *Rapid Commun. Mass Spectr.* 25, 3563–3574. doi: 10.1002/rcm.5251
- Zeng, Y. B., Ward, D. M., Brassell, S. C., and Eglinton, G. (1992). Biogeochemistry of hot spring environments: 2. Lipid compositions of Yellowstone (Wyoming, USA) cyanobacterial and *Chloroflexus* mats. *Chem. Geol.* 95, 327–345.
- Zhang, C. L., Ye, Q., Huang, Z., Li, W., Chen, J., Song, Z., et al. (2008). Global occurrence of archaeal amoA genes in terrestrial hot springs. *Appl. Environ. Microbiol.* 74, 6417–6426. doi: 10.1128/AEM.00843-08
- Zhang, X., Ferguson-Miller, S. M., and Reid, G. E. (2009). Characterization of ornithine and glutamine lipids extracted from cell membranes of *Rhodobacter sphaeroides*. *J. Am. Soc. Mass Spectr.* 20, 198–212. doi: 10.1016/j.jasms.2008.08.017
- Zhou, A., Chiu, B. K., Weber, Y., Elling, F. J., Cobban, A. B., Pearson, A., et al. (2019). Energy flux controls tetraether lipid cyclization in *Sulfolobus acidocaldarius*. *Environ. Microbiol.* 22, 343–353. doi: 10.1111/1462-2920.14851

Conflict of Interest: The authors declare that the research was conducted in the absence of any commercial or financial relationships that could be construed as a potential conflict of interest.

Copyright © 2020 Boyer, Schubotz, Summons, Woods and Shock. This is an open-access article distributed under the terms of the Creative Commons Attribution License (CC BY). The use, distribution or reproduction in other forums is permitted, provided the original author(s) and the copyright owner(s) are credited and that the original publication in this journal is cited, in accordance with accepted academic practice. No use, distribution or reproduction is permitted which does not comply with these terms.